

Hybrid Energy Storage and Applications Based on High Power Pulse Transformer Charging

Yu Zhang and Jinliang Liu

Additional information is available at the end of the chapter

<http://dx.doi.org/10.5772/52217>

1. Introduction

1.1. HES based on pulse transformer charging

In the fields of electrical discipline, power electronics and pulsed power technology, the common used modes of energy transferring and energy storage include mechanical energy storage (MES), chemical energy storage (CHES), capacitive energy storage (CES), inductive energy storage (IES) and the hybrid energy storage (HES) [1-3]. The MES and CHES are important ways for energy storage employed by people since the early times. The MES transfers mechanical energy to pulse electromagnetic energy, and the typical MES devices include the generator for electricity. The CHES devices, such as batteries, transfer the chemical energy to electrical energy. The energy storage modes aforementioned usually combine with each other to form an HES mode. In our daily life, the MES and CHES usually need the help of other modes to deliver or transfer energy to drive the terminal loads. As a result, CES, IES and HES become the most important common used energy storage modes for users. So, these three energy storage modes are analyzed in detail as the central topics in this chapter.

The CES is an energy storage mode employing capacitors to store electrical energy [3-5]. As Fig. 1(a) shows, C_0 is the energy storage component in CES, and the load of C_0 can be inductors, capacitors and resistors respectively. Define the permittivity of dielectric in capacitor C_0 as ε , the electric field intensity of the stored electrical energy in C_0 as E . The energy density W_E of CES is as

$$W_E = \frac{1}{2} \varepsilon E^2 . \quad (1)$$

Usually, W_E which is restricted to ε and the breakdown electric field intensity of C_0 is about $10^4 \sim 10^5 \text{ J/m}^3$. The traditional Marx generators are in the CES mode [4-5].

The IES is another energy storage mode using inductive coils to generate magnetic fields for energy storage. As shown in Fig. 1(b), the basic IES cell needs matched operations of the opening switch (S_{open}) and the closing switch (S_{close}) [6-7], while L_0 is as the energy storage component. When the charging current of L_0 reaches its peak, S_{open} becomes open and S_{close} becomes closed at the same time. As the instantaneously induced voltage on L_0 grows fast, the previously stored magnetic energy in the magnetic field is delivered fast to the load through S_{close} . The load of L_0 also can respectively be inductors, capacitors and resistors. The explosive magnetic flux compression generator is a kind of typical IES device [7]. The coil winding of pulse transformer which has been used in Tokamak facility is another kind of important IES device [8]. Define the permeability of the medium inside the coil windings as μ , the magnetic induction intensity of the stored magnetic energy as B . The energy density W_B of IES is as

$$W_B = \frac{1}{2} \frac{B^2}{\mu} \quad (2)$$

Usually, W_B restricted by μ and B is about 10^7 J/m^3 . IES has many advanced qualities such as high density of energy storage, compactness, light weight and small volume in contrast to CES. However, disadvantages of IES are also obvious, such as requirement of high power opening switches, low efficiency of energy transferring and disability of repetitive operations.

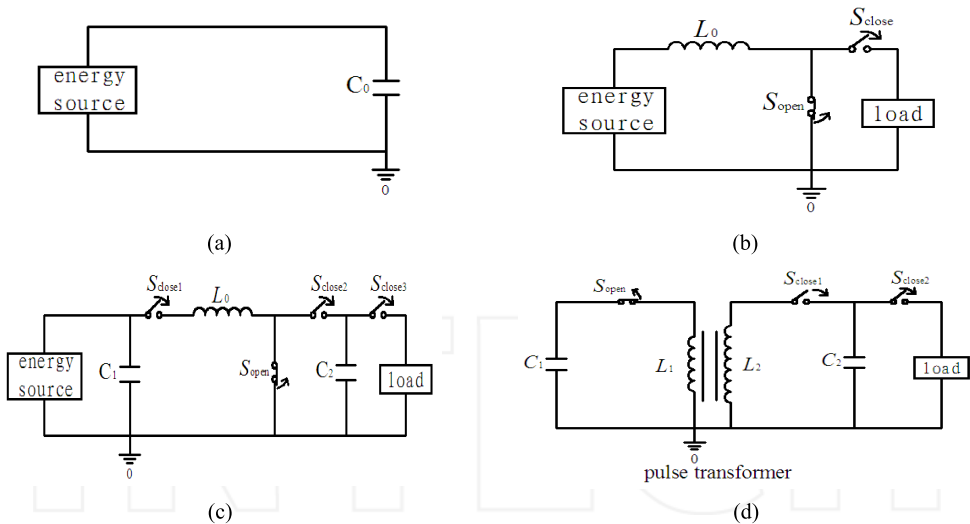


Figure 1. Schematics of three kinds of common-used energy storage modes. (a) Capacitive energy storage mode; (b) Inductive energy storage mode; (c) Typical hybrid energy storage mode; (d) Hybrid energy storage based on pulse transformer.

In many applications, CES combining with IES is adopted for energy storage as a mode of HES. Fig. 1(c) shows a typical HES mode based on CES and IES. Firstly, the energy source charges C_1 in CES mode. Secondly, S_{close1} closes and the energy stored in C_1 transfers to L_0

through the resonant circuit in IES mode. Thirdly, the previously closed switch S_{open} opens, and S_{close2} closes at the same time. The accumulated magnetic energy in L_0 transfers fast to capacitor C_2 in CES mode again. Finally, S_{close3} closes and the energy stored in C_2 is delivered to the terminal load. So, in the HES mode shown in Fig. 1(c), the HES cell orderly operates in CES, IES and CES mode to obtain high power pulse energy. Furthermore, the often used HES mode based on CES and IES shown in Fig. 1(d) is a derivative from the mode in Fig. 1(c). In this HES mode, pulse transformer is employed and the transformer windings play as IES components. In Fig. 1(d), if S_{open} and S_{close1} operate in order, the HES cell also orderly operates in CES, IES and CES mode. Of course, switch S_{close1} in Fig. 1(d) also can be ignored in many applications for simplification.

Generally speaking, a system can be called as HES module if two or more than two energy storage modes are included in the system. In this chapter, the centre topics just focus on CES, IES and the HES based on the CES and IES, as they have broad applications in our daily life. The CES and IES both have their own advantages and defects, but the HES mode based on these two achieves those individual advantages at the same time. In applications, a lot of facilities can be simplified as the HES module including two capacitors and a transformer shown in Fig. 2 [9-16]. Switch S_1 has ability of closing and opening at different time. This kind of HES module based on transformer charging can orderly operate in CES, IES and CES mode. And it has many improved features for application at the same time, such as high efficiency of energy transferring, high density of energy storage and compactness.

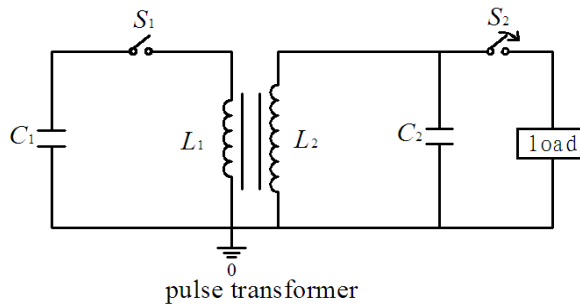


Figure 2. Schematic of the common used hybrid energy storage mode based on capacitors and pulse transformer

1.2. Applications of HES based on pulse transformer charging

The HES based on pulse transformer charging is an important technology for high-voltage boosting, high-power pulse compression, pulse modification, high-power pulse trigger, intense electron beam accelerator and plasma source. The HES cell has broad applications in the fields such as defense, industry, environmental protection, medical care, physics, cell biology and pulsed power technology.

The HES based on pulse transformer charging is an important way for high-power pulse compression. Fig. 3(a) shows a high-power pulse compression facility based on HES in

Nagaoka University of Technology in Japan [9], and its structure is shown in Fig. 3(b). The Blumlein pulse forming line plays as the load capacitor in the HES cell, and two magnetic switches respectively control the energy transferring. The pulse compression system can compress the low voltage pulse from millisecond range to form high voltage pulse at 50ns/480kV range.

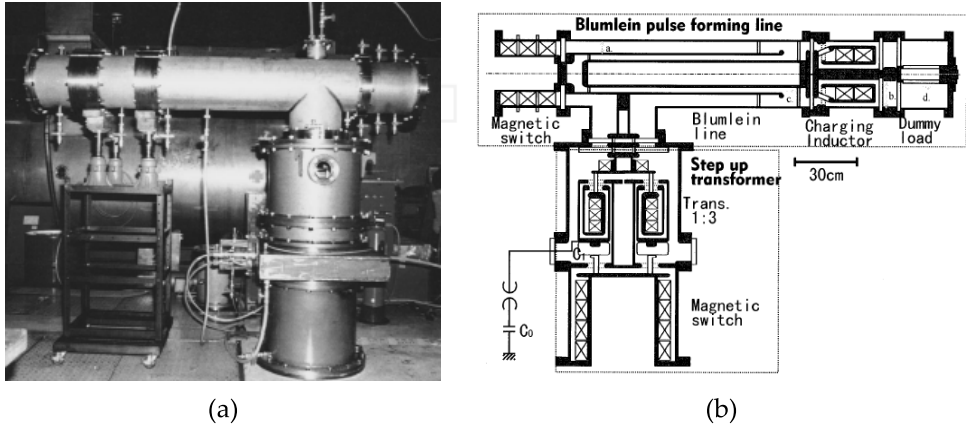


Figure 3. Typical high power pulse compressor with a transformer-based HES module. (a) The pulse compressor system; (b) the diagram and schematic of the pulse compressor system

The HES based on pulse transformer charging is an important way for high-power pulse trigger. Fig. 4(a) shows a solid state pulse trigger with semiconductor opening switches (SOS) in the Institute of Electrophysics Russian Academy of Science [10-11]. Fig. 4(b) presents the schematic of the pulse trigger, which shows a typical HES mode based on pulse transformer charging. SOS switch and IGBT are employed as the switches controlling energy transferring. The pulse trigger delivers high-voltage trigger pulse with pulse width at 70ns and voltage ranging from 20 to 80kV under the 100Hz repetition. And the average power delivered is about 50kW.

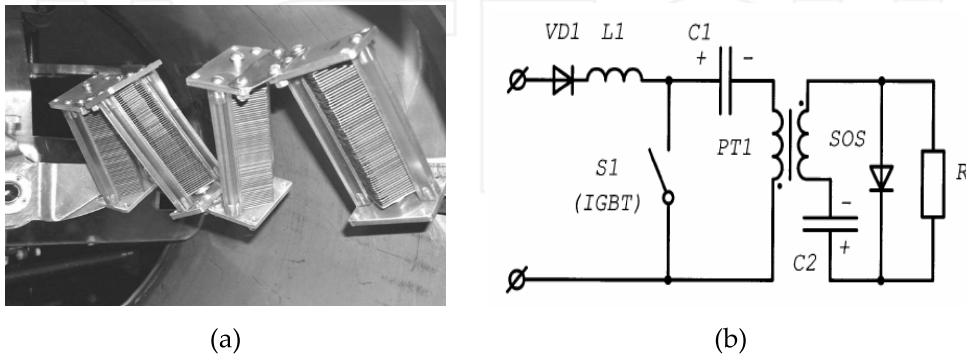


Figure 4. Typical high-voltage narrow pulse trigger with the transformer-based HES module. (a) The pulse trigger with the SOS switches; (b) The schematic of the high-power pulse trigger system

The HES cell based on pulse transformer charging is also an important component in intense electron beam accelerator for high-power pulse electron beams which are used in the fields of high-power microwave, plasma, high-power laser and inertial fusion energy (IFE). Fig. 5(a) shows the “Sinus” type accelerator in Russia [12], and it also corresponds to the HES mode based on transformer charging shown in Fig. 2. The pulse transformer of the accelerator is Tesla transformer with opened magnetic core, while spark gap switch controls energy transferring. The accelerator has been used to drive microwave oscillator for high-power microwave. Fig. 5(b) presents a high-power KrF laser system in Naval Research Laboratory of the U. S. A., and the important energy storage components in the system just form an HES cell based on transformer charging [13-14]. The HES cell drives the diode for pulse electron beams to pump the laser, and the laser system delivers pulse laser with peak power at 5GW/100ns to the IFE facility.

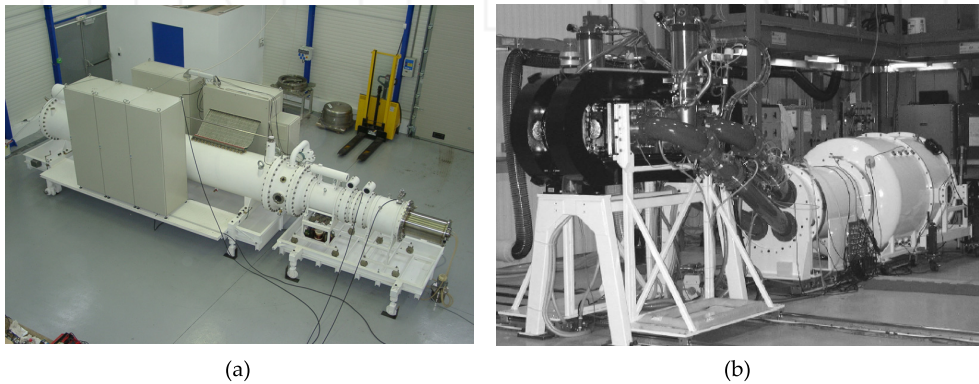


Figure 5. Typical intense electron beam accelerator with the transformer-based HES module. (a) The pulse electron beam accelerator based on HES for high-power microwave application in Russia; (b) The pulse electron beam accelerator based on HES for high-power laser application in Naval Research Laboratory, the U. S. A.

The HES based on pulse transformer charging also have important applications in ultra-wideband (UWB) electromagnetic radiation and X-ray radiography. Fig. 6 shows an ultra-wideband pulse generator based HES mode in Loughborough University of the U. K. [15]. The air-core Tesla transformer charges the pulse forming line (PFL) up to 500kV, and spark gap switch controls the energy transferring form the PFL to antenna. The “RADAN” series pulse generators shown in Fig. 7 are portable repetitive high-power pulsers made in Russia for X-ray radiography [16]. The “RADAN” pulser which consists of Tesla transformer and PFL are also based on the HES mode shown in Fig. 2. The controlling switches are thyristors and spark gap.

Besides, the HES cell is also used in shockwave generator [17], dielectric barrier discharge [18], industrial exhaust processing [19], material surface treatment [20], ozone production [21], food sterilization [22], cell treatment and cell mutation [23].

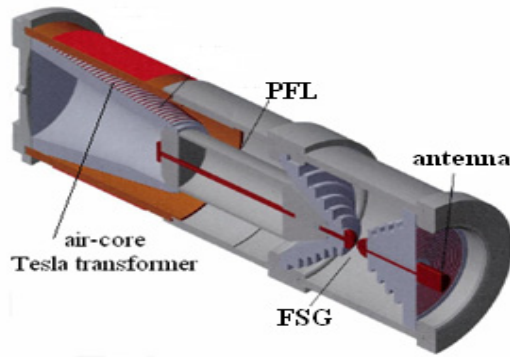


Figure 6. Compact 500kV pulse generator based on HES for UWB radiation in Loughborough University, U. K.

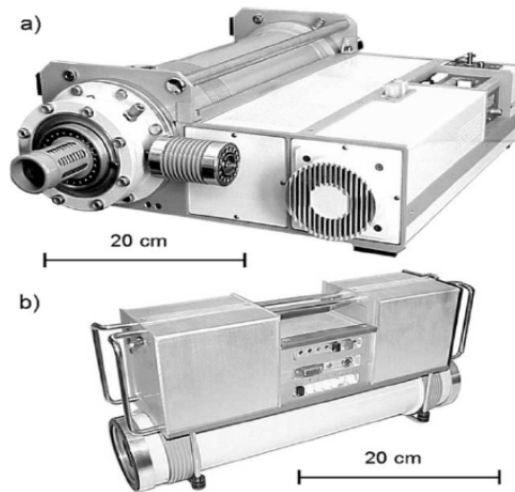


Figure 7. The compact “RADAN” pulse generators for X-ray radiography in Russia

2. Parametric analysis of pulse transformer with closed magnetic core in HES

Capacitor and inductor are basic energy storage components for CES and IES respectively, and pulse transformer charging is important to the HES mode shown in Fig. 2. So, it is essential to analyze the characteristic parameters of the common used high-power pulse transformer, and provide theoretical instructions for better understanding of the HES based on transformer charging.



Figure 8. Common used pulse transformers with closed toroidal magnetic cores

There are many kinds of standards for categorizing the common used pulse transformers. From the perspective of magnetic core, pulse transformers can be divided into two types, such as the magnetic-core transformer [24-25] and the air-core transformer [26]. In view of the geometric structures of windings, the pulse transformer can be divided to many types, such as pulse transformer with closed magnetic core, solenoid-winding transformer, curled spiral strip transformer [26], the cone-winding Tesla transformer [16, 27], and so on. The transformer with magnetic core is preferred in many applications due to its advantages such as low leakage inductance, high coupling coefficient, high step-up ratio and high efficiency of energy transferring. Russian researchers produced a kind of Tesla transformer with cone-like windings and opened magnetic core, and the transformer with high coupling coefficient can deliver high voltage at MV range in repetitive operations [27]. Usually, pulse transformer with closed magnetic core, as shown in Fig.8, is the typical common used transformer which has larger coupling coefficient than that of Tesla transformer. The magnetic core can be made of ferrite, electrotechnical steel, iron-based amorphous alloy, nano-crystallization alloy, and so on. The magnetic core is also conductive so that the core needs to be enclosed by an insulated capsule to keep insulation from transformer windings.

Paper [28] presents a method for Calculation on leakage inductance and mutual inductance of pulse transformer. In this chapter, the common used pulse transformer with toroidal magnetic core will be analyzed in detail for theoretical reference. And a more convenient and simple method for analysis and calculation will be presented to provide better understanding of pulse transformer [24-25].

The typical geometric structure of pulse transformer with toroidal magnetic core is shown in Fig. 9(a). The transformer consists of closed magnetic core, insulated capsule of the core and transformer windings. The cross section of the core and capsule is shown in Fig. 9(b). Transformer windings are formed by high-voltage withstanding wires curling around the capsule, and turn numbers of the primary and secondary windings are N_1 and N_2 ,

respectively. Usually, transformer windings have a layout of only one layer of wires as shown in Fig. 9(a), which corresponds to a simple structure. In other words, this simple structure can be viewed as a single-layer solenoid with a circular symmetric axis in the azimuthal direction. The transformer usually immerses in the transformer oil for good heat sink and insulation.

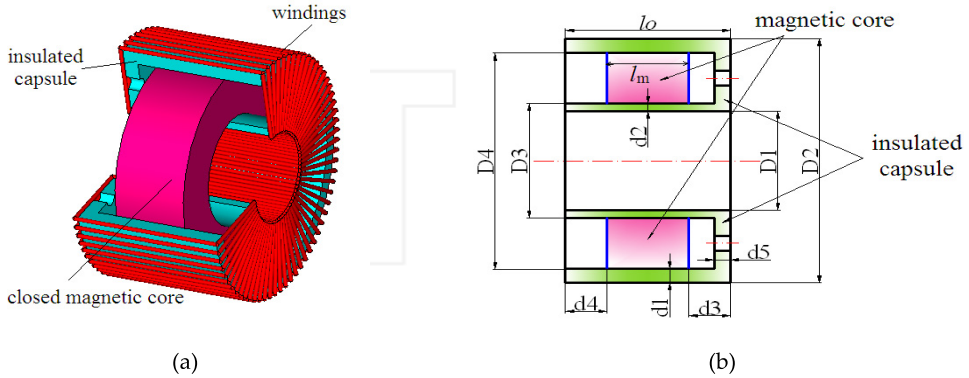


Figure 9. Typical structure of the pulse transformer with a closed magnetic core and an insulated capsule. (a) Assembly structure of the pulse transformer; (b) Geometric structure of the cross section of the pulse transformer.

Define the geometric parameters in Fig. 9(b) as follows. The height, outer diameter and inner diameter of the closed magnetic core are defined as l_m , D_4 and D_3 respectively. The height, outer diameter and inner diameter of the insulated capsule are defined as l_0 , D_2 and D_1 respectively. The thicknesses of the outer wall, inner wall and side wall of insulated capsule are defined as d_1 , d_2 and d_5 in order. The distances between the side surfaces of capsule and magnetic core are d_3 and d_4 shown in Fig. 9(b). Define diameters of wires of the primary windings and secondary windings as d_p and d_s respectively. The intensively wound primary windings with N_1 turns have a width about $N_1 d_p$.

2.1. Inductance analysis of pulse transformer windings with closed magnetic core

2.1.1. Calculation of magnetizing inductance

Define the permittivity and permeability of free space as ϵ_0 and μ_0 , relative permeability of magnetic core as μ_r , the saturated magnetic induction intensity of core as B_s , residue magnetic induction intensity of core as B_r , and the filling factor of magnetic core as K_r . The cross section area S of the core is as

$$S = (D_4 - D_3)l_m / 2. \tag{3}$$

Define the inner and outer circumferences of magnetic core as l_1 and l_2 , then $l_1 = \pi D_3$ and $l_2 = \pi D_4$. The primary and secondary windings tightly curl around the insulated capsule in

separated areas in the azimuthal direction. In order to get high step-up ratio, the turn number N_1 of primary windings is usually small so that the single-layer layout of primary windings is in common use. Define the current flowing through the primary windings as i_p , the total magnetic flux in the magnetic core as Φ_0 , and the magnetizing inductance of transformer as L_μ . According to Ampere's circuital law,

$$\Phi_0 = i_p \mu_0 \mu_r N_1^2 S K_T \ln(l_2 / l_1) / (l_2 - l_1) \quad (4)$$

As $\Phi_0 = L_\mu i_p$, L_μ is obtained as

$$L_\mu = \frac{\mu_0 \mu_r N_1^2 S K_T \ln(l_2 / l_1)}{l_2 - l_1}. \quad (5)$$

2.1.2. Leakage inductance of primary windings

The leakage inductances of primary and secondary windings also contribute to the total inductances of windings. The leakage inductance L_{ip} of the primary windings is caused by the leakage magnetic flux outside the magnetic core. If μ_r of magnetic core is large enough, the solenoid approximation can be used. Through neglecting the leakage flux in the outside space of the primary windings, the leakage magnetic energy mainly exists in two volumes. As Fig.10 shows, the first volume defined as V_1 corresponds to the insulated capsule segment only between the primary windings and the magnetic core, and the second volume defined as V_2 is occupied by the primary winding wires themselves. The leakage magnetic field in the volume enclosed by transformer windings can be viewed in uniform distribution. The leakage magnetic energy stored in V_1 and V_2 are as W_{m1} and W_{m2} , respectively.

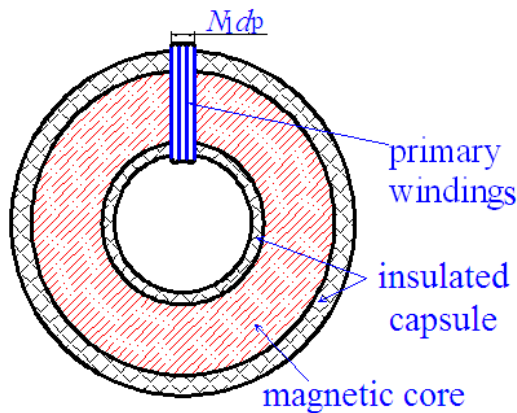


Figure 10. Primary windings structure of pulse transformer with closed magnetic core.

Define the magnetic field intensity generated by i_p from the N_1 -turn primary windings as H_p in V_1 . According to Ampere's circuital law, $H_p \approx i_p / d_p$. From Fig. 10,

$$V_1 = N_1 l_0 d_p (d_1 + d_2) + (D_4 - D_3) N_1 d_p (d_4 + d_3) / 2. \quad (6)$$

When the magnetic core works in the linear district of its hysteresis loop, the magnetic energy W_{m1} stored in V_1 is as

$$W_{m1} = \frac{\mu_0}{2} H_p^2 V_1 = \frac{\mu_0}{2} \left(\frac{i_p}{d_p}\right)^2 V_1. \quad (7)$$

In V_2 , the leakage magnetic field intensity defined as H_{px} can be estimated as

$$H_{px} = \frac{i_p}{d_p} \frac{x}{d_p}, \quad 0 \leq x \leq d_p. \quad (8)$$

From the geometric structure in Fig. 10, $V_2 = 2N_1 d_p^2 (l_0 + (D_2 - D_1) / 2)$, the leakage magnetic energy W_{m2} stored in V_2 is as

$$W_{m2} = \frac{1}{2} \mu_0 \int_0^{d_p} d(V_2 H_{px}^2) = \frac{\mu_0 V_2}{2} \frac{i_p^2}{3d_p^2}. \quad (9)$$

So, the total leakage magnetic energy W_{mp} stored in V_1 and V_2 is presented as

$$W_{mp} = W_{m1} + W_{m2} = L_{lp} i_p^2 / 2 \quad (10)$$

In (10), L_{lp} is the leakage inductance of the primary windings, and L_{lp} can be calculated as

$$L_{lp} = \frac{\mu_0}{3d_p^2} (V_2 + 3V_1). \quad (11)$$

2.1.3. Leakage inductance of secondary windings

Usually, the simple and typical layout of the secondary windings of transformer is also the single layer structure as shown in Fig. 11(a). The windings are in single-layer layout both at the inner wall and outer wall of insulated capsule. As D_2 is much larger than D_1 , the density of wires at the inner wall is larger than that at the outer wall. However, if the turn number N_2 becomes larger enough for higher step-up ratio, the inner wall of capsule can not provide enough space for the single-layer layout of wires while the outer wall still supports the previous layout, as shown in Fig. 11(b). We call this situation as “quasi-single-layer” layout. In the “quasi-single-layer” layout shown in Fig. 11 (b), the wires at the inner wall of capsule is in two-layer layout. After wire 2 curls in the inner layer, wire 3 curls in the outer layer next to wire 2, and wire 4 curls in the inner layer again next to wire 3, then wire 5 curls in the outer layer again next to wire 4, and so on. This kind of special layout has many

advantages, such as minor voltage between adjacent coil turns, uniform voltage distribution between two layers, good insulation property and smaller distributed capacitance of windings.

In this chapter, the single-layer layout and “quasi-single-layer” layout shown in Fig. 11 (a) and (b) respectively are both analyzed to provide reference for HES module. And the multi-layer layout [29] can also be analyzed by the way introduced in this chapter.

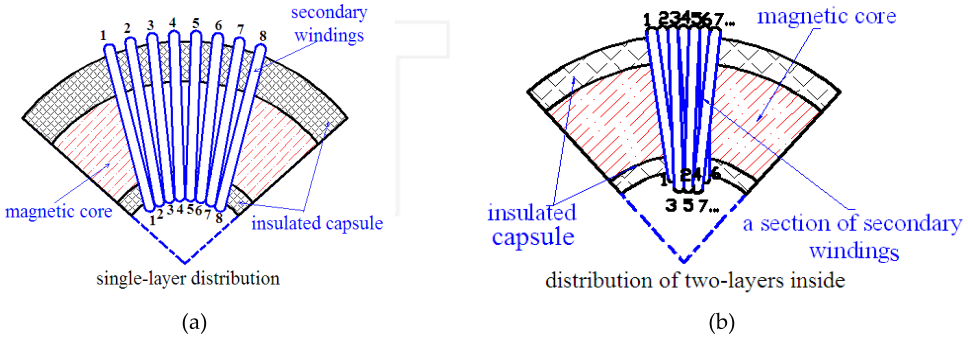


Figure 11. Secondary windings structures of pulse transformer with closed magnetic core. (a) Single-layer distribution of the secondary windings of transformer; (b) Inter-wound “quasi-single-layer” distribution of the secondary windings

Define the current flowing through the secondary windings as i_s , the two volumes storing leakage magnetic energy as V_a and V_b , the corresponding leakage magnetic energy as W_{ma} and W_{mb} , the total leakage magnetic energy as W_{ms} , wire diameter of secondary windings as d_s , and the leakage inductance of secondary windings as L_{ls} .

Firstly, the single-layer layout shown in Fig. 11 (a) is going to be analyzed. The analytical model is similar to the model analyzed in Fig. 10. If $(D_2 - D_1) \ll D_1$, the length of leakage magnetic pass enclosed by the secondary windings is as $l_{ms} = N_2 d_s (D_2 + D_1) / 2(D_1 - d_s)$. The leakage magnetic field intensity defined as H_s in V_a is presented as $H_s = N_2 i_s / l_{ms}$. V_a and W_{ma} can be estimated as

$$\begin{cases} V_a = \frac{N_2 d_s}{4(D_1 - d_s)} [l_0 (D_2^2 - D_1^2) - l_m \pi (D_4^2 - D_3^2)] \\ W_{ma} = \frac{\mu_0}{2} \frac{N_2^2 i_s^2}{l_{ms}^2} V_a \end{cases} \quad (12)$$

In volume V_b which is occupied by the secondary winding wires themselves, W_{mb} can be estimated as

$$W_{mb} = \frac{1}{2} \mu_0 \int_0^{d_s} (H_s \frac{x}{d_s})^2 l_{ms} (2l_0 + 4d_s + D_2 - D_1) dx = \frac{\mu_0 d_s N_2^2 i_s^2}{3l_{ms}} [l_0 + 2d_s + (D_2 - D_1) / 2]. \quad (13)$$

In view of that $W_{ms} = W_{ma} + W_{mb} = L_{ls}i_s^2 / 2$, the leakage inductance of single-layer layout of the secondary windings is as

$$L_{ls} = \frac{\mu_0 N_2^2 V_a}{l_{ms}^2} + \frac{2\mu_0 d_s N_2^2}{3l_{ms}} [l_0 + 2d_s + (D_2 - D_1) / 2] \quad (14)$$

As to the “quasi-single-layer” layout shown in Fig. 11 (b), it also can be analyzed by calculating the leakage magnetic energy firstly. Under this condition, the length of leakage magnetic pass enclosed by the secondary windings is revised as $l_{ms} \approx N_2 d_s (D_2 + D_1) / 4(D_1 - d_s)$. The leakage magnetic energy W_{ma} and W_{mb} can be estimated as

$$\left\{ \begin{array}{l} W_{ma} = \frac{\mu_0 N_2^2 i_s^2}{2} \frac{V_a}{l_{ms}^2} \\ W_{mb} = \frac{1}{2} \mu_0 \int_0^{d_s} (H_s \frac{x}{d_s})^2 [\pi(D_2 + d_s)(l_0 + 2d_s) + \pi(D_1 - d_s)(l_0 + 2d_s) + \\ \quad + \pi(D_1 - 3d_s)(l_0 + 2d_s) + \pi(D_2^2 - D_1^2) / 2] dx \\ \quad = \frac{\mu_0 \pi N_2^2 i_s^2 d_s}{6d_s^2} [(l_0 + 2d_s)(D_2 + 2D_1 - 3d_s) + (D_2^2 - D_1^2) / 2] \end{array} \right. \quad (15)$$

Finally, the leakage inductance of the “quasi-single-layer” layout is obtained by the same way of (14) as

$$L_{ls} = \frac{\mu_0 N_2^2}{l_{ms}^2} V_a + \frac{\mu_0 \pi N_2^2 d_s}{2d_s^2} [(l_0 + 2d_s)(D_2 + 2D_1 - 3d_s) + (D_2^2 - D_1^2) / 2]. \quad (16)$$

2.1.4. The winding inductances of pulse transformer

Define the total inductances of primary windings and secondary windings as L_1 and L_2 respectively, the mutual inductance of the primary and secondary windings as M , and the effective coupling coefficient of transformer as K_{eff} . From (5), (11), (14) or (16),

$$\left\{ \begin{array}{l} L_1 = L_\mu + L_{ps} \\ L_2 = L_\mu (N_2 / N_1)^2 + L_{ss} \end{array} \right. \quad (17)$$

When $\mu_r \gg 1$, M and K_{eff} are presented as

$$\left\{ \begin{array}{l} M = L_\mu N_2 / N_1 \\ K_{eff} = \frac{M}{\sqrt{L_1 L_2}} = \sqrt{1 - \frac{L_{ps} + L_{ss} (N_1 / N_2)^2}{L_\mu}} \end{array} \right. \quad (18)$$

2.2. Distributed capacitance analysis of pulse transformer windings

The distributed capacitances of pulse transformer include the distributed capacitances to ground [30], capacitance between adjacent turns or layers of windings [29-32], and capacitance between the primary and secondary windings [32-33]. It is very difficult to accurately calculate every distributed capacitance. Even if we can do it, the results are not liable to be analyzed so that the referential value is discounted. Under some reasonable approximations, lumped capacitances can be used to substitute the corresponding distributed capacitances for simplification, and more useful and instructive results can be obtained [29]. Of course, the electromagnetic dispersion theory can be used to analyze the lumped inductance and lumped capacitance of the single-layer solenoid under different complicated boundary conditions [34-35]. In this section, an easier way is introduced to analyze and estimate the lumped capacitances of transformer windings.

2.2.1. Distributed capacitance analysis of single-layer transformer windings

In the single-layer layout of transformer windings shown in Fig. 11(a), the equivalent schematic of transformer with distributed capacitances is shown in Fig. 12. C_{Dpi} is the distributed capacitance between two adjacent coil turns of primary windings, and C_{Dsi} is the counterpart capacitance of the secondary windings. C_{psi} is the distributed capacitance between primary and secondary windings. Common transformers have distributed capacitances to the ground, but this capacitive effect can be ignored if the distance between transformer and ground is large. If the primary windings and secondary windings are viewed as two totalities, the lumped parameters C_{Dp} , C_{Ds} and C_{ps} can be used to substitute the "sum effects" of C_{Dpi} , C_{Dsi} and C_{psi} in order, respectively. And the lumped schematic of the pulse transformer is also shown in Fig. 12. C_{ps} decreases when the distance between primary and secondary windings increases. In order to retain good insulation for high-power pulse transformer, this distance is usually large so that C_{ps} also can be ignored. At last, only the lumped capacitances, such as C_{Dp} and C_{Ds} , have strong effects on pulse transformer.

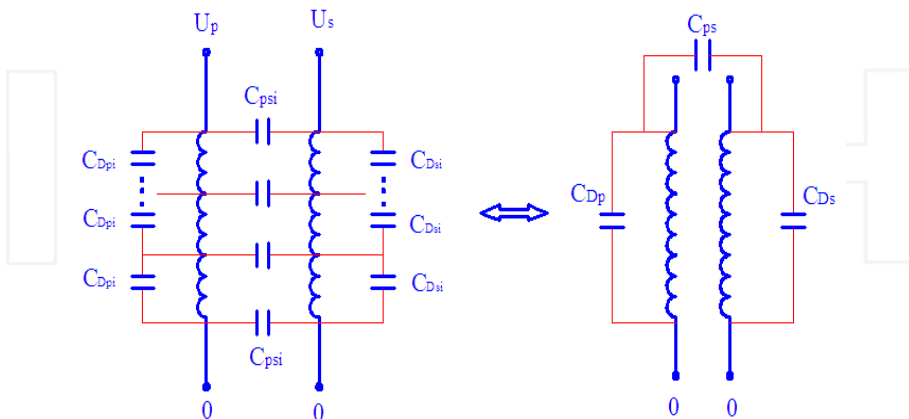


Figure 12. The distributed capacitances of single-layer wire-wound pulse transformer and the equivalent schematic with lumped parameters

In the single-layer layout shown in Fig. 11(a), define the lengths of single coil turn in primary and secondary windings as l_{s1} and l_{s2} respectively, the face-to-face areas between two adjacent coil turns in primary and secondary windings as S_{w1} and S_{w2} respectively, and the distances between two adjacent coil turns in primary and secondary windings as Δd_p and Δd_s respectively. According to the geometric structures shown in Fig. 10 and Fig. 11(a), $l_{s1}=2l_0+4d_p+D_2-D_1$, $l_{s2}=2l_0+4d_s+D_2-D_1$, $S_{w1}=d_p l_{s1}$ and $S_{w2}=d_s l_{s2}$. Because the coil windings distribute as a sector, Δd_p and Δd_s both increase when the distance from the centre point of sector increases in the radial direction. Δd_p and Δd_s can be estimated as

$$\Delta d_p(r) = \frac{2N_1 d_p r}{(N_1 - 1)(D_1 - d_p)}, \quad \Delta d_s(r) = \frac{2N_2 d_s r}{(N_2 - 1)(D_1 - d_s)}, \quad \frac{D_1}{2} < r < \frac{D_2}{2}. \quad (19)$$

If the relative permittivity of the dielectric between adjacent coil turns is ε_r , C_{Dpi} and C_{Dsi} can be estimated as

$$\left\{ \begin{array}{l} C_{Dpi} = \int_{\frac{D_1}{2}}^{\frac{D_2}{2}} \frac{\varepsilon_0 \varepsilon_r S_{w1} (N_1 - 1)(D_1 - d_p) dr}{2N_1 d_p r^2} = \frac{\varepsilon_0 \varepsilon_r l_{s1} (N_1 - 1)(D_1 - d_p)(D_2 - D_1)}{N_1 D_1 D_2} \\ C_{Dsi} = \int_{\frac{D_1}{2}}^{\frac{D_2}{2}} \frac{\varepsilon_0 \varepsilon_r S_{w2} (N_2 - 1)(D_1 - d_s) dr}{2N_2 d_s r^2} = \frac{\varepsilon_0 \varepsilon_r l_{s2} (N_2 - 1)(D_1 - d_s)(D_2 - D_1)}{N_2 D_1 D_2} \end{array} \right. \quad (20)$$

Actually, the whole long coil wire which forms the primary or secondary windings of transformer can be viewed as a totality. The distributed capacitances between adjacent turns are just formed by the front surface and the back surface of the wire totality itself. In view of that, lumped capacitances C_{Dp} and C_{Ds} can be used to describe the total distributed capacitive effect. As a result, C_{Dp} and C_{Ds} are calculated as

$$\left\{ \begin{array}{l} C_{Dp} = \int_0^{(N_1-1)l_{s1}} d_p dl_{s1} \int_{\frac{D_1}{2}}^{\frac{D_2}{2}} \frac{\varepsilon_0 \varepsilon_r (N_1 - 1)(D_1 - d_p) dr}{2N_1 d_p r^2} = \frac{\varepsilon_0 \varepsilon_r l_{s1} (N_1 - 1)^2 (D_1 - d_p)(D_2 - D_1)}{N_1 D_1 D_2} \\ \quad = (N_1 - 1)C_{Dpi} \\ C_{Ds} = \int_0^{(N_2-1)l_{s2}} d_s dl_{s2} \int_{\frac{D_1}{2}}^{\frac{D_2}{2}} \frac{\varepsilon_0 \varepsilon_r (N_2 - 1)(D_1 - d_s) dr}{2N_2 d_s r^2} = \frac{\varepsilon_0 \varepsilon_r l_{s2} (N_2 - 1)^2 (D_1 - d_s)(D_2 - D_1)}{N_2 D_1 D_2} \\ \quad = (N_2 - 1)C_{Dsi} \end{array} \right. \quad (21)$$

From (21), C_{Dp} or C_{Ds} is proportional to the wire length l_{s1} or l_{s2} , while larger turn number and smaller distance between adjacent coil turns both cause larger C_{Dp} or C_{Ds}

2.2.2. Distributed capacitance analysis of inter-wound “quasi-single-layer” windings

Usually, large turn number N_2 corresponds to the “quasi-single-layer” layout of wires shown in Fig. 13(a). In this situation, distributed capacitances between the two layers of

wires at the inner wall of capsule obviously exist. Of course, lumped capacitance C_{Ls} can be used to describe the capacitive effect when the two layers are viewed as two totalities, as shown in Fig. 13(b). Define C_{Ds1} and C_{Ds2} as the lumped capacitances between adjacent coil turns of these two totalities, and C_{Ds} is the sum when C_{Ds1} and C_{Ds2} are in series. As a result, the lumped capacitances which have strong effects on pulse transformer are C_{Dp} , C_{Ds1} , C_{Ds2} and C_{Ls} .

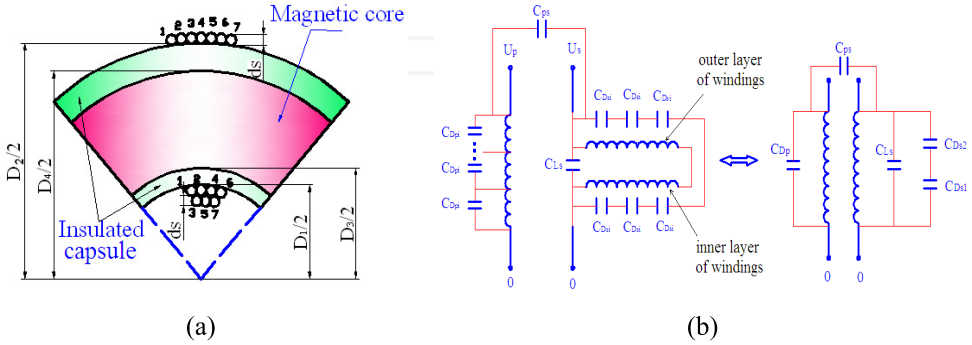


Figure 13. The distributed capacitances of “quasi-single-layer” pulse transformer and the equivalent schematic with lumped parameters. (a) Double-layer inside distribution of the secondary windings; (b) Equivalent circuit of transformer with distributed capacitances and lumped parameters

If the coil turns are tightly wound, the average distance between two adjacent coil turns is d_s . The inner layer and outer layer at the inner wall of capsule have coil numbers as $1+N_2/2$ and $N_2/2-1$ respectively. According to the same way for (21), C_{Ds1} and C_{Ds2} are obtained as

$$\begin{cases} C_{Ds1} = \frac{\varepsilon_0 \varepsilon_r l_{s2} (N_2 / 2 + 1)^2 (D_1 - d_s) (D_2 - D_1)}{(N_2 / 2) D_1 D_2} \\ C_{Ds2} = \frac{\varepsilon_0 \varepsilon_r (l_{s2} + 3d_s) (N_2 / 2 - 1)^2 (D_1 - d_s) (D_2 - D_1)}{(N_2 / 2) D_1 D_2} \end{cases} \quad (22)$$

The non-adjacent coil turns have large distance so that the capacitance effects are shielded by adjacent coil turns. In the azimuthal direction of the inner layer wires, small angle $d\theta$ corresponds to the azimuthal width of wires as dl and distributed capacitance as dC_{Ls} . Then, $dC_{Ls} = \frac{\varepsilon_0 \varepsilon_r (D_2 - D_1 + 5d_s + 2l_0)}{2d_s} dl$. If the voltage between the $(n-1)$ th and n th turn of coil ($n \leq$

N_2) is ΔU_0 , the inter-wound method of the two layers aforementioned retains the voltage between two layers at about $2\Delta U_0$. So, the electrical energy W_{Ls} stored in C_{Ls} between the two layers is as

$$W_{Ls} = \frac{1}{2} \int_1^{N_2} (2\Delta U_0)^2 dC_{Ls} = \Delta U_0^2 \varepsilon_0 \varepsilon_r N_2 (D_2 - D_1 + 5d_s + 2l_0) / 2. \quad (23)$$

In view of that $W_{Ls}=C_{Ls}(2\Delta U_0)^2/2$, C_{Ls} can be calculated as

$$C_{Ls} = \frac{\varepsilon_0 \varepsilon_r (D_2 - D_1 + 5d_s + 2l_0) N_2}{4} \quad (24)$$

According to the equivalent lumped schematic in Fig. 13(b), the total lumped capacitance C_{Ds} can be estimated as

$$C_{Ds} = \frac{1}{1/C_{Ds1} + 1/C_{Ds2}} + C_{Ls} \quad (25)$$

2.3. Dynamic resistance of transformer windings

Parasitic resistance and junction resistance of transformer windings cause loss in HES cell. Define the resistivity of winding wires under room temperature (20°C) as ρ_0 , the work temperature as T_w , resistivity of winding wires under T_w as $\rho(T_w)$, radius of the conductive section of wire as r_w , total wire length as l_w , and the static parasitic resistance of winding wires as R_{w0} . The empirical estimation for R_{w0} is as

$$R_{w0} = \rho(T_w) \frac{l_w}{\pi r_w^2} = \rho_0 [1 + 0.004(T_w - 20)] \frac{l_w}{\pi r_w^2} \quad (26)$$

When the working frequency f is high, the “skin effect” of current flowing through the wire cross-section becomes obvious, which has great effects on R_{w0} . Define the depth of “skin effect” as Δd_w , and the dynamic parasitic resistance of winding wires as $R_w(f, T_w)$. As $\Delta d_w = (\rho / \pi f \mu_0)^{0.5}$, $R_w(f, T_w)$ is presented as

$$R_w(f, T_w) = \begin{cases} \frac{l_w}{(2r_w - \frac{\rho(T_w)}{\pi f \mu_0}) \sqrt{\frac{\pi}{f \mu_0 \rho(T_w)}}}, & r_w > \Delta d_w \\ R_{w0} = \rho(T_w) \frac{l_w}{\pi r_w^2}, & r_w \leq \Delta d_w \end{cases} \quad (27)$$

3. Pulse response analysis of high power pulse transformer in HES

In HES cell based on pulse transformer charging, the high-frequency pulse response characteristics of transformer show great effects on the energy transferring and energy storage. Pulse response and frequency response of pulse transformer are very important issues. The distributed capacitances, leakage inductances and magnetizing inductance have great effects on the response pulse of transformer with closed magnetic core [36-39]. In this Section, important topics such as the frequency response and pulse response characteristics to square pulse, are discussed through analyzing the pulse transformer with closed magnetic core.

3.1. Frequency-response analysis of pulse transformer with closed magnetic core

The equivalent schematic of ideal pulse transformer circuit is shown in Fig. 14(a). L_{lp} and L_{ls} are the leakage inductances of primary and secondary windings of transformer calculated in (11), (14) and (16). Lumped capacitances C_{ps} , C_{DP} and C_{Ds} represent the “total effect” of the distributed capacitances of transformer, while C_{DP} and C_{Ds} are calculated in (21) and (25). L_{μ} is the magnetizing inductance of pulse transformer calculated in (5). Define the sum of wire resistance of primary windings and the junction resistance in primary circuit as R_p , the counterpart resistance in secondary circuit as R_s , load resistance as R_L , the equivalent loss resistance of magnetic core as R_c , and the sinusoidal/square pulse source as U_1 .

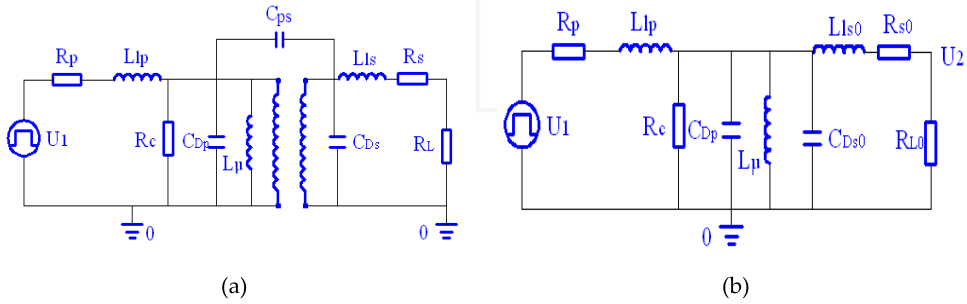


Figure 14. Equivalent schematics of pulse transformer based on magnetic core with a square pulse source and a load resistor. (a) Equivalent schematic of pulse transformer with all the distributed parameters; (b) Simplified schematic of pulse transformer when the secondary circuit is equated into the primary circuit.

Usually, C_{ps} is so small that it can be ignored due to the enough insulation distance between the primary and secondary windings. In order to simplify the transformer circuit in Fig. 14(a), the parameters in the secondary circuit such as C_{Ds} , L_{ls} , R_s and R_L , can be equated into the primary circuit as C_{Ds0} , L_{ls0} , R_{s0} and R_{L0} , respectively. And the equating law is as

$$\begin{cases} L_{ls0} = L_{ls} \left(\frac{N_1}{N_2} \right)^2, & C_{Ds0} = C_{Ds} \left(\frac{N_2}{N_1} \right)^2 \\ R_{s0} = R_s \left(\frac{N_1}{N_2} \right)^2, & R_{L0} = R_L \left(\frac{N_1}{N_2} \right)^2 \end{cases} \quad (28)$$

3.1.1. Low-frequency response characteristics

Define the frequency and angular frequency of the pulse source as f and ω_0 . When the transformer responds to low-frequency pulse signal ($f < 10^3$ Hz), Fig. 14(b) can also be simplified. In Fig. 14(b), C_{DP} is in parallel with C_{Ds0} , and the parallel combination capacitance of these two is about $10^{-6} \sim 10^{-9}$ F so that the reactance can reach $10 \text{ k}\Omega \sim 1 \text{ M}\Omega$. Meanwhile, the reactance of L_{μ} is small. As a result, C_{DP} and C_{Ds0} can also be ignored. Reactances of L_{ls0} and

L_{lp} ($10^{-7}H$) are also small under the low-frequency condition, and they also can be ignored. Usually, the resistivity of magnetic core is much larger than common conductors to restrict eddy current. In view of that $R_{s0} \ll R_{L0} \ll R_c$, the combination of R_{s0} , R_{L0} and R_c can be substituted by R_0 . Furthermore, $R_0 \cong R_{L0}$. Finally, the equivalent schematic of pulse transformer under low-frequency condition is shown in Fig.15(a).

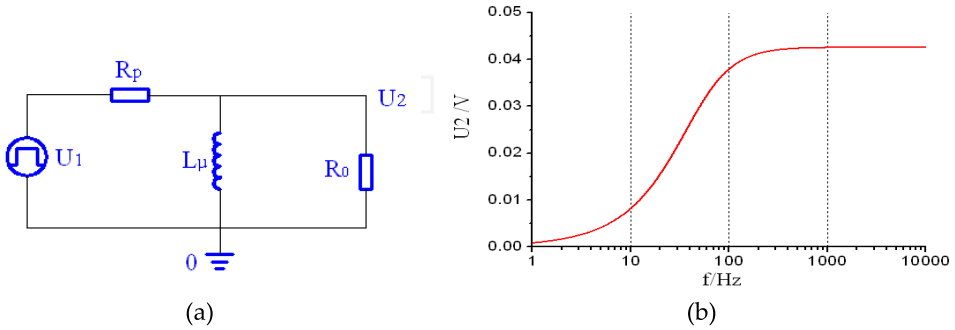


Figure 15. Simplified schematic and analytical result of transformer for low-frequency pulse response. (a) Equivalent schematic of pulse transformer under the condition of low frequency; (b) Low-frequency response results of an example of transformer

In Fig. 15(a), L_{μ} and R_0 are in parallel, and then in series with R_p which is at $m\Omega$ range. R_0 is usually very small due to the equating process from (28). When ω_0 of the pulse source increases, reactance of L_{μ} also increases so that $\omega_0 L_{\mu} \gg R_0$. In this case, the L_{μ} branch gets close to opening, and an ideal voltage divider is formed only consisting of R_p and R_0 . At last, the pulse source U_1 is delivered to the load R_0 without any deformations. And the response voltage pulse signal U_2 of transformer on the load resistor is as

$$U_2 = U_1 \frac{R_0}{R_0 + R_p} \tag{29}$$

When $R_p \ll R_0$, $U_1 = U_2$ which means the source voltage completely transfers to the load resistor. On the other hand, if $\omega_0 L_{\mu} \ll R_0$, L_{μ} shares the current from the pulse source so that the current flowing through R_0 gets close to 0. In this situation, the pulse transformer is not able to respond to the low-frequency pulse signal U_1 .

An example is provided as follows to demonstrate the analysis above. In many measurements, coaxial cables and oscilloscope are used, and the corresponding terminal impedance is about $R_t = 50\Omega$. So, the R_0 may be at $m\Omega$ range when it is equated to the primary circuit. Select conditions as follows: $R_p = 0.09\Omega$, $L_{\mu} = 12.6\mu H$, and U_1 is the periodical sinusoidal voltage pulse with amplitude at 1V. The low-frequency response curve of pulse transformer is obtained from Pspice simulation on frequency scanning, as Fig. 15(b) shows. When f of U_1 is larger than the second inflexion frequency (100Hz), response signal U_2 is large and stable. However, when f is less than the first inflexion frequency (10Hz), response signal U_2 gets close to 0. And the cut-off frequency f_c is about 10Hz.

The conclusion is that low-frequency response capability of pulse transformer is mainly determined by L_{μ} , and the response capability can be improved through increasing L_{μ} calculated in (5).

3.1.2. High-frequency response characteristics

When the transformer responds to high-frequency pulse signal ($f > 10^6$ Hz), conditions “ $\omega_0 L_{\mu} \gg R_0$ ” and “ $\omega_0 L_{\mu} \gg R_p$ ” are satisfied so that the branch of L_{μ} seems open. In Fig. 14(b), the combination effect of R_{s0} , R_{L0} and R_c still can be substituted by R_0 . Substitute L_{lp} and L_{ls0} by L_l , and combine C_{Ds0} and C_{Dp} as C_D . The simplified schematic of pulse transformer for high-frequency response is shown in Fig. 16(a).

In Fig. 16(a), when ω_0 of pulse source increases, reactance of L_l increases while reactance of C_D decreases. If ω_0 is large enough, $\omega_0 L_l \gg R_0 \gg 1/(\omega_0 C_D)$ and the response signal U_2 gets close to 0. On the other hand, condition $1/(\omega_0 C_D) \geq R_0$ is satisfied when ω_0 decreases. The pulse current mainly flows through the load resistor R_0 , and the good response of transformer is obtained. Especially, when $\omega_0 L_l \ll R_p$, L_l also can be ignored. Under this situation, R_p is in series with R_0 again, and the response signal U_2 which corresponds to the best response still conforms to (29).

Select the amplitude of the periodical pulse signal U_1 at 1V. If R_p , L_l and C_D are at ranges of mΩ, 0.1μH and pF respectively, the high-frequency response curve of transformer is also obtained as shown in Fig.16(b) from Pspice simulation. When f is less than the first inflexion frequency (about 300kHz), response signal U_2 is stable. When f is larger than the second inflexion frequency (about 10MHz), response signal U_2 gets close to 0. And the cut-off frequency f_H is about 10MHz.

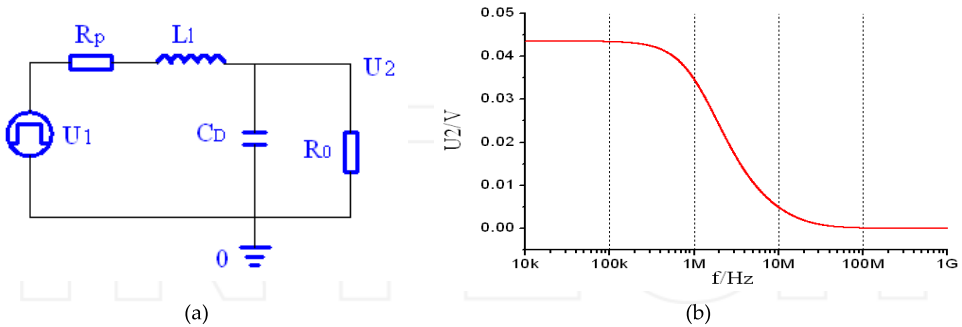


Figure 16. Simplified schematic and analytical result of transformer for high-frequency pulse response. (a) Equivalent schematic of pulse transformer under the condition of high frequency; (b) High-frequency response results of an example of transformer

The conclusion is that high-frequency response characteristics of transformer are mainly determined by distributed capacitance C_D and leakage inductance L_l . The high-frequency

response characteristics can be obviously improved through restricting C_D and L_μ , or increasing L_μ .

3.2. Square pulse response of pulse transformer with closed magnetic core

In Fig. 14(b), $R_{s0} \ll R_{L0} \ll R_c$, and the combination effect of R_{s0} , R_{L0} and R_c can be substituted by R_0 . Combine $C_{D_{s0}}$ with C_{D_p} as C_D . The simplified schematic of pulse transformer circuit for square pulse response is shown in Fig. 17. U_1 and U_2 represent the square voltage pulse source and the response voltage signal on the load respectively. The total current from the pulse source is $i(t)$, while the branch currents flowing through R_0 , C_D and L_μ are as i_1 , i_2 and i_3 respectively.

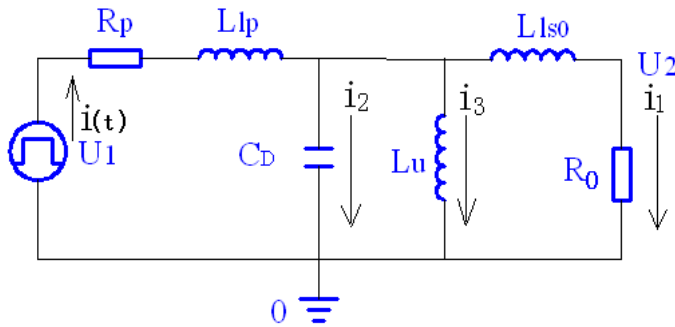


Figure 17. Equivalent schematic of transformer for square pulse response

3.2.1. Response to the front edge of square pulse

Usually, L_μ ranges from $10^{-6}H$ up to more than $10^{-5}H$, and the square pulse has front edge and back edge both at $100ns \sim 1\mu s$ range. So, when the fast front edge and back edge of square pulse appear, reactance of L_μ is much larger than the equated load resistor R_0 . Under this condition, i_3 is so small that the effect of L_μ on the front edge response can be ignored.

Define the voltage of C_D as $U_c(t)$. As aforementioned, L_μ has little effect on the response to the front edge of square pulse. Through Ignoring the L_μ branch, the circuit equations are presented in (30) with initial conditions as $i(0)=0$, $i_1(0)=0$ and $U_c(0)=0$.

$$\begin{cases} U_1(t) = i(t)R_p + L_{lp} \frac{di(t)}{dt} + L_{ls0} \frac{di_1(t)}{dt} + i_1(t)R_0 \\ L_{ls0} \frac{di_1(t)}{dt} + i_1(t)R_0 = \int i_2(t) dt / C_D \\ i(t) = i_1(t) + i_2(t) \end{cases} \quad (30)$$

If the factor for Laplace transformation is as p , the transformed forms of $U_1(t)$ and $i_1(t)$ are defined as $U_1(p)$ and $I_1(p)$. Firstly, four constants such as α , β , γ and λ are defined as

$$\left\{ \begin{array}{l} \alpha = \frac{R_p L_{ls0} C_D + R_0 L_p C_D}{L_{lp} L_{ls0} C_D}, \beta = \frac{R_0 R_p C_D + L_{lp} + L_{ls0}}{L_{lp} L_{ls0} C_D} \\ \gamma = \frac{R_p + R_0}{L_{lp} L_{ls0} C_D}, \lambda = \frac{1}{L_{lp} L_{ls0} C_D} \end{array} \right. \quad (31)$$

Define the amplitude and pulse duration of square voltage pulse source as U_s and T_0 respectively. $U_1(t)$ is as

$$U_1(t) = \begin{cases} 0, & t < 0 \text{ or } t \geq T_0 \\ U_s, & 0 \leq t < T_0 \end{cases} \quad (32)$$

Equations (30) can be solved by Laplace transformation and convolution, and there are three states of solutions such as the over dumping state, the critical dumping state and the under dumping state. In the transformer circuit, the resistors are always small so that the under dumping state usually appears. Actually, the under dumping state is the most important state which corresponds to the practice. In this section, the centre topic focuses on the under dumping state of the circuit.

Define constants a, b, ω, ξ ($a, b < 0; \omega > 0$), A_1, A_2 and A_3 as (33).

$$\left\{ \begin{array}{l} A_1 = \frac{1}{(a-b)^2 + \omega^2}, A_2 = \frac{-1}{(a-b)^2 + \omega^2}, A_3 = \frac{2b-a}{(a-b)^2 + \omega^2} \\ a = \xi^{\frac{1}{3}} - \xi^{-\frac{1}{3}}(3\beta - \alpha^2)/9 - \alpha/3 \\ b = \xi^{-\frac{1}{3}}(3\beta - \alpha^2)/18 - \alpha/3 - \xi^{\frac{1}{3}}/2 \\ \omega = \sqrt{3}[(3\beta - \alpha^2)\xi^{-\frac{1}{3}}/9 + \xi^{\frac{1}{3}}]/2 \\ \xi \triangleq \sqrt{\frac{\beta^3 + \alpha^3\gamma}{27} - \frac{\alpha^2\beta^2}{108} - \frac{\alpha\beta\gamma}{6} + \frac{\gamma^2}{4} - \frac{3\gamma - \alpha\beta}{6} - \frac{\alpha^3}{27}} \end{array} \right. \quad (33)$$

The under dumping state solution of (30) is as

$$U_2(t) = \begin{cases} 0, & t \leq 0 \\ \lambda R_0 U_s \{A_1 \exp(at) + [A_2 \cos(\omega t) + (A_2 b + A_3) \sin(\omega t) / \omega] \exp(bt)\}, & 0 < t \leq T_0 \\ \lambda U_s R_0 \{A_1 \exp(at) + [A_2 \cos(\omega t) + (A_2 b + A_3) \sin(\omega t) / \omega] \exp(bt)\} - \lambda U_s R_0 \{A_1 \exp[a(t - T_0)] + [A_2 \cos \omega(t - T_0) + (A_2 b + A_3) \sin \omega(t - T_0) / \omega] \exp[b(t - T_0)]\}, & t > T_0 \end{cases} \quad (34)$$

The load current $i_1(t) = U_2(t)/R_0$. From (34), response voltage pulse $U_2(t)$ on load consists of an exponential damping term and a resonant damping term. The resonant damping term which has main effects on the front edge of pulse contributes to the high-frequency resonance at the front edge. Constant a defined in (33) is the damping factor of the pulse

droop of square pulse $U_2(t)$, b is the damping factor of the resonant damping term, and ω is the resonant angular frequency. Substitute $\lambda R_0 U_s$ by U_0 , and define two functions $f_1(t)$ and $f_2(t)$ as

$$f_1(t) = \begin{cases} 0, & t \leq 0 \\ U_0[A_2 \cos(\omega t) + (A_2 b + A_3) \sin(\omega t) / \omega] \exp(bt), & 0 < t \leq T_0 \\ U_0[A_2 \cos(\omega t) + (A_2 b + A_3) \sin(\omega t) / \omega] \exp(bt) - U_0 \\ [A_2 \cos \omega(t - T_0) + (A_2 b + A_3) \sin \omega(t - T_0) / \omega] \exp[b(t - T_0)], & t > T_0 \end{cases} \quad (35)$$

$$f_2(t) = U_0[A_2 \cos(\omega t) + (A_2 b + A_3) \sin(\omega t) / \omega]$$

$f_1(t)$ is just the resonant damping term divided from (34), while $f_2(t)$ is the pure resonant signal divided from $f_1(t)$. If pulse width $T_0=5\mu\text{s}$, the three signals $U_2(t)$, $f_1(t)$ and $f_2(t)$ are plotted as Curve 1, Curve 2 and Curve 3 in Fig. 18 respectively. In the abscissa of Fig. 18, the section when $t < 0$ corresponds to the period before the time when the square pulse appears. Obviously, Curve 1~ Curve 3 all have high-frequency resonances with the same angular ω . The resonances of Curve 1 and Curve 2 at the front edge are in superposition. Under the under damping state of the circuit, the rise time t_r of the response signal is about half of a resonant period as (36).

$$t_r = \pi / \omega. \quad (36)$$

From (33) and (36), the rise time of the response signal $U_2(t)$ is determined by the parasitic inductance, leakage inductances (L_{lp} and L_{ls0}) and distributed capacitance C_D . The rise time t_r of the front edge can be minimized through increasing the resonant angular frequency ω . In the essence, the high-frequency “L-C-R” resonance is generated by the leakage inductances and distributed capacitance in the circuit.

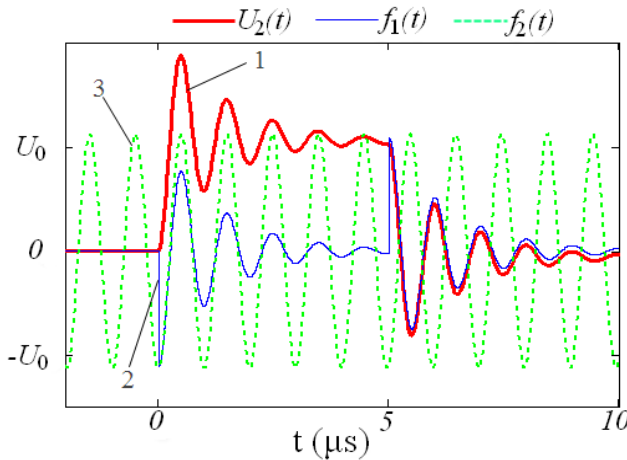


Figure 18. Typical pulse response waveforms of pulse transformer to the front edge of square pulse

The conclusion is that the rise time of the front edge of response pulse can be improved by minimizing the capacitance C_D and leakage inductance L_{lp} and L_{ls0} of the transformer. The waveform of the response voltage signal can be improved through increasing the damping resistor of the circuit in a proper range.

3.2.2. Pulse droop analysis of transformer response

In Fig.17, when the front edge of pulse is over, $U_c(t)$ of C_D and the currents flowing through L_{lp} and L_{ls0} all become stable. And these parameters have little effects on the response to the flat top of square pulse. During this period, load voltage signal $U_2(t)$ is mainly determined by L_μ . So, the simplified schematic from Fig.17 is shown as Fig.19 (a). The circuit equations are as

$$\begin{cases} U_1(t) = i(t)R_p + i_1(t)R_0 \\ U_2(t) = i_1(t)R_0 = L_\mu di_3(t) / dt. \\ i(t) = i_1(t) + i_3(t) \end{cases} \quad (37)$$

The initial conditions are as $i_3(0)=0$ and $U_2(0)=R_0U_s/(R_0+R_p)$. The load voltage $U_2(t)$ is obtained as (38) through solving equations in (37).

$$U_2(t) = \frac{R_0U_s}{R_p + R_0} \exp\left(-\frac{t}{\tau}\right), \quad \tau = \frac{L_\mu(R_p + R_0)}{R_pR_0}, \quad 0 < t < T_0. \quad (38)$$

In (38), τ is the constant time factor of the pulse droop. When L_μ increases which leads to an increment of τ , the pulse droop effect is weakened and the pulse top becomes flat. If $U_{20}=R_0U_s/(R_p+R_0)$, the response signal to the flat top of square pulse is shown in Fig. 19(b). When pulse duration T_0 is short at μs range, the pulse droop effect ($0 < t < T_0$) of $U_2(t)$ is not obvious at all. However, when T_0 ranges from 0.1ms to several milliseconds, time factor τ has great effect on the flat top of $U_2(t)$, and the pulse droop effect of the response signal is so obvious that $U_2(t)$ becomes an triangular wave.

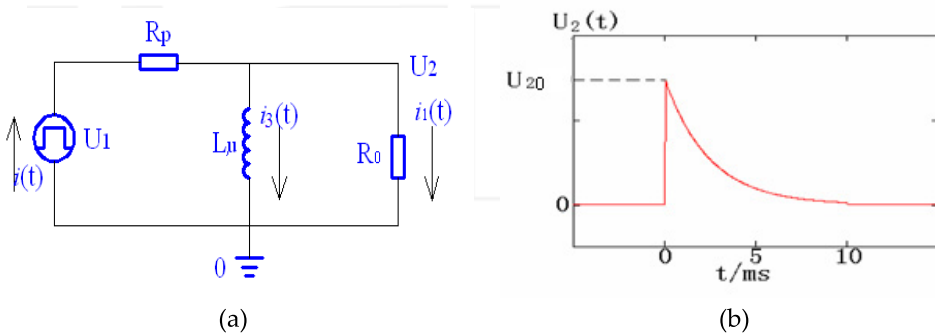


Figure 19. Schematic and response pulse of transformer to the flat-top of square pulse. (a) Equivalent schematic of transformer for flat top response of square pulse; (b) The pulse droop of the response pulse of transformer

3.2.3. Response to the back edge of square pulse

When the flat top of square pulse is over, all the reactive components in Fig. 17 have stored certain amount of electrical or magnetic energy. Though the main pulse of the response signal is over, the stored energy starts to deliver to the load through the circuit. As a result, high-frequency resonance is generated again which has a few differences from the resonance at the front edge of pulse. In Fig. 17, U_1 and R_p have no effects on the pulse tail response when the main pulse is over. C_D which was charged plays as the voltage source. Combine L_{lp} and L_{ls0} as L_l . The equivalent schematic for pulse tail response of transformer is shown in Fig. 20.

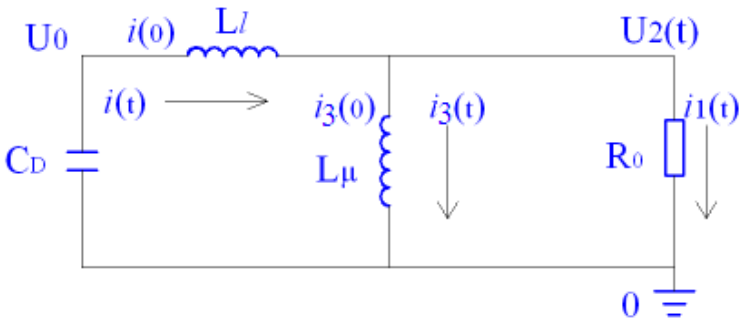


Figure 20. Equivalent schematic for back edge response of transformer to square pulse

The circuit equations are presented in (39) with initial condition as $U_c(0)=U_{c0}$.

$$\begin{cases} U_{c,0} - \int i(t)dt / C_D = L_l di(t) / dt + i_1(t)R_0 \\ U_2(t) = i_1(t)R_0 = L_\mu di_3(t) / dt \\ i(t) = i_1(t) + i_3(t) \end{cases} \quad (39)$$

$i_1(0)$ and $i_3(0)$ are determined by the final state of the pulse droop period. There are also three kinds of solutions, however the under damping solution usually corresponds to the real practices. So, this situation is analyzed as the centre topic in this section. Define six constants $\alpha_1, \beta_1, \gamma_1, \alpha_2, \beta_2$ and γ_2 as (40).

$$\begin{cases} \alpha_1 = \frac{R_0}{L_\mu} + \frac{R_0}{L_l}, \beta_1 = \frac{1}{L_l C_D}, \gamma_1 = \frac{R_0}{L_l L_\mu C_D} \\ \alpha_2 = R_0[i(0) - i_2(0)], \beta_2 = \frac{R_0 U_0}{L_l}, \gamma_2 = -\frac{R_0 i_2(0)}{L_l C_D} \end{cases} \quad (40)$$

The under damping solution of (39) is calculated as

$$U_2(t) = B_1 \exp(a_1 t) + \exp(b_1 t) \left[B_2 \cos(\omega_s t) + \frac{B_2 b_1 + B_3}{\omega_s} \sin(\omega_s t) \right]. \quad (41)$$

In (41), B_1 , B_2 and B_3 are three coefficients while a_1 , b_1 , ω_s and ξ_1 are another four constants as

$$\left\{ \begin{array}{l} B_1 = \frac{\alpha_2 a_1^2 + \beta_2 a_1 + \gamma_2}{(a_1 - b_1)^2 + \omega_s^2}, B_2 = \alpha_2 - \frac{\alpha_2 a_1^2 + \beta_2 a_1 + \gamma_2}{(a_1 - b_1)^2 + \omega_s^2}, B_3 = \frac{(\alpha_2 a_1^2 + \beta_2 a_1 + \gamma_2)(b_1^2 + \omega_s^2)}{a_1 [(a_1 - b_1)^2 + \omega_s^2]} - \frac{\gamma_2}{a_1} \\ a_1 = \xi_1^{\frac{1}{3}} - \xi_1^{-\frac{1}{3}} (3\beta_1 - \alpha_1^2) / 9 - \alpha_1 / 3 \\ b_1 = \xi_1^{\frac{1}{3}} (3\beta_1 - \alpha_1^2) / 18 - \alpha_1 / 3 - \xi_1^{-\frac{1}{3}} / 2 \\ \omega_s = \sqrt{3} [(3\beta_1 - \alpha_1^2) \xi_1^{\frac{1}{3}} / 9 + \xi_1^{-\frac{1}{3}}] / 2 \\ \xi_1 \triangleq \sqrt{\frac{\beta_1^3 + \alpha_1^3 \gamma_1}{27} - \frac{\alpha_1^2 \beta_1^2}{108} - \frac{\alpha_1 \beta_1 \gamma_1}{6} + \frac{\gamma_1^2}{4} - \frac{3\gamma_1 - \alpha_1 \beta_1}{6} - \frac{\alpha_1^3}{27}} \end{array} \right. \quad (42)$$

The responses to front edge and back edge of square pulse have differences in essence, as the exciting sources are different. Define functions $f_3(t)$ and $f_4(t)$ as (43), according to (41).

$$\left\{ \begin{array}{l} f_3(t) = B_1 \exp(a_1 t) \\ f_4(t) = \exp(b_1 t) \left[B_2 \cos(\omega_s t) + \frac{B_2 b_1 + B_3}{\omega_s} \sin(\omega_s t) \right] \end{array} \right. \quad (43)$$

The response signal $U_2(t)$ in (41) also consists of an exponential damping term $f_3(t)$ and a resonant damping term $f_4(t)$.

Define $B_1 + B_2$ as U_0' . In order to help to establish direct impressions, a batch of parameters are selected ($C_D = 2.14 \mu\text{F}$, $L_\mu = 12.6 \mu\text{H}$ and $L_r = 1.09 \mu\text{H}$) for plotting the response pulse curves. According to (41) and (43), signals $U_2(t)$, $f_3(t)$ and $f_4(t)$ are plotted as Curve 1, Curve 2 and Curve 3 respectively in Fig. 21(a) for example. Because the damping factor a_1 defined in (42) is large, the amplitude of $f_3(t)$ which corresponds to Curve 2 is very small with slow damping. The resonant damping term $f_4(t)$ which is damped faster determines the resonant angular frequency ω_s . The resonant parts of $U_2(t)$ and $f_4(t)$ are also in superposition at the back edge of pulse. When $f_4(t)$ is damped to 0, $U_2(t)$ becomes the same as $f_3(t)$. The half of the resonant period t_d is as

$$t_d = \pi / \omega_s. \quad (44)$$

According to (40) and (42), R_0 has effects on the damping factors of $f_3(t)$ and $f_4(t)$. The resonant frequency is mainly determined by leakage inductance, magnetizing inductance and distributed capacitance of transformer.

Fig. 21(b) shows an impression of the effect of L_μ on the tail of response signal. When L_μ changes from $0.1 \mu\text{H}$ to 1mH while other parameters retain the same, the resonant

waveforms with the same frequency do not have large changes. So, the conclusion is that, t_d and the resonant angular frequency ω_s are not mainly determined by L_μ . Fig. 21(c) shows the effect of leakage inductances of transformer on the pulse tail of response signal. When L_l is small at 10nH range, the back edge of pulse (Curve 2) is good as which of standard square pulse. When L_l increases from 0.01 μ H to 1 μ H range, the resonances become fierce with large amplitudes. If L_l increases to 10 μ H range, the previous under damping mode has a transition close to the critical damping mode (Curve 4). The fall time t_d of the pulse tail increases obviously. Fig. 21(d) shows the effect of distributed capacitances of transformer on the pulse tail of response signal. The effect of C_D obeys similar laws obtained from L_μ . So, the conclusion is that the pulse tail of the response signal can be improved by a large extent through minimizing the leakage inductances and distributed capacitances of transformer windings. Paper [24] demonstrated the analysis above in experiments.

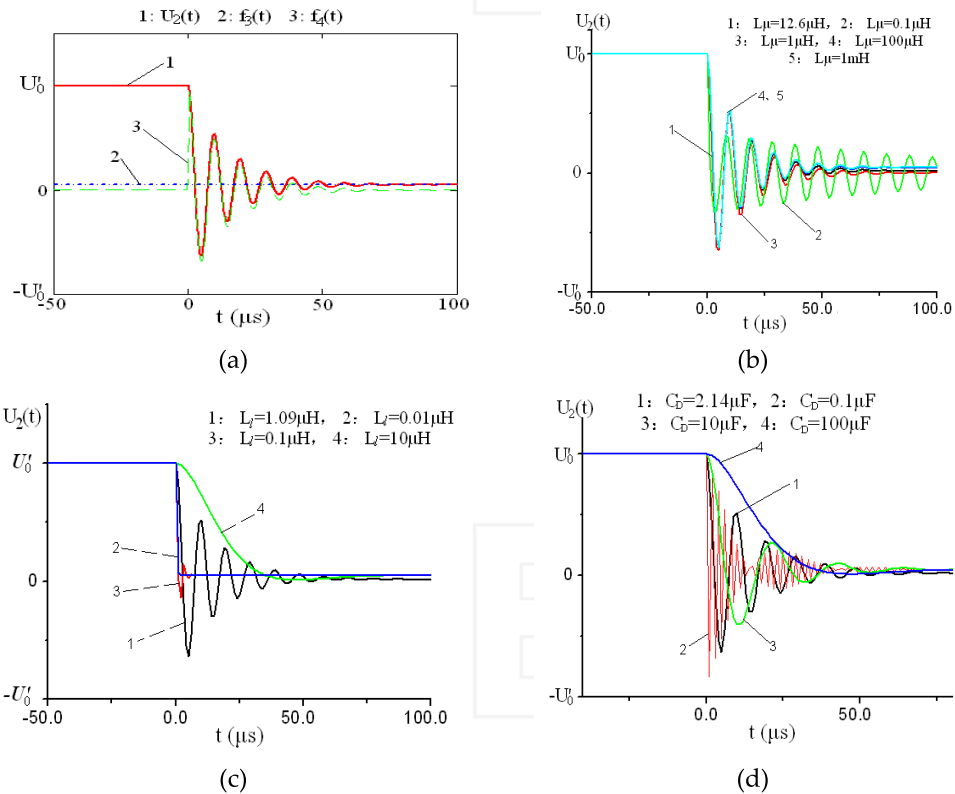


Figure 21. Typical back tail response signals of pulse transformer to the square pulse. (a) The typical back edge response signals to square pulse in theory; (b) Effects of magnetizing inductance on the back edge response of transformer; (b) Effects of leakage inductance on the back edge response of transformer; (c) Effects of distributed capacitance on the back edge response of transformer;

4. Analysis of energy transferring in HES based on pulse transformer charging

As an important IES component, the pulse transformer is analyzed and the pulse response characteristics are also discussed in detail. The analytical theory aforementioned is the base for HES analysis based on pulse transformer charging in this section. In Fig. 2, the HES module based on capacitors and transformer operates in three courses, such as the CES course, the IES course and the CES course. Actually, the IES course and the latter CES course occur almost at the same time. The pulse transformer plays a role on energy transferring. There are many kinds of options for the controlling switch (S_1) of C_1 , such as mechanical switch, vacuum trigger switch, spark gap switch, thyristor, IGBT, thyatron, photo-conductive switch, and so on. S_1 has double functions including opening and closing. S_1 ensures the single direction of HES energy transferring, from C_1 and transformer to C_2 . In this section, the energy transferring characteristics of HES mode based on transformer charging is analyzed in detail.

The pulse signals in the HES module are resonant signals. According to the analyses from Fig. 15 and Fig.16, the common used pulse transformer shown in Fig. 9(a) has good frequency response capability in the band ranging from several hundred Hz to several MHz. Moreover, C_1 and C_2 in HES module are far larger than the distributed capacitances of pulse transformer. So, the distributed capacitances can be ignored in HES cell. In the practical HES module, many other parameters should be considered, such as the junction inductance, parasitic inductance of wires, parasitic inductance of switch, parasitic resistance of wires, parasitic resistance of switch, and so on. These parameters can be concluded into two types as the parasitic inductance and parasitic resistance. As a result, the equivalent schematic of the HES module is shown in Fig. 22(a).

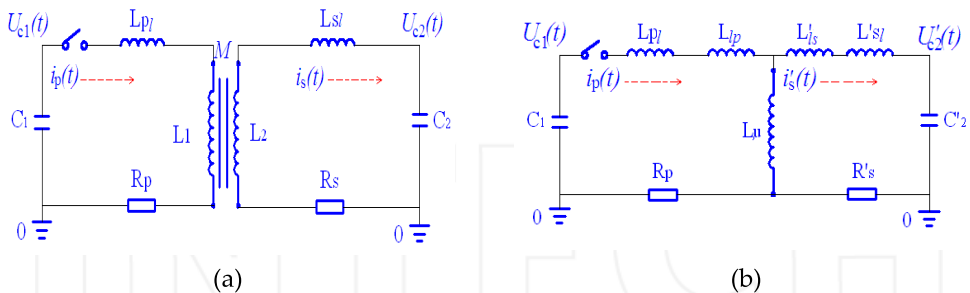


Figure 22. The basic hybrid energy storage (HES) system based on a source capacitor, a pulse transformer and a load capacitor. (a) Typical schematic of the transformer-based HES module; (b) Simplified schematic when the secondary circuit is equated into the primary circuit

In Fig. 22(a), C_1 and C_2 represent the primary energy-storage capacitor and load capacitor respectively. L_{pl} and L_{sl} represent the parasitic inductances in the primary circuit and secondary circuit, while R_p and R_s stand for the parasitic resistances in the primary circuit and secondary circuit respectively. L_1 , L_2 and M of transformer are defined in (17) and (18). $i_p(t)$ and $i_s(t)$ represent the current in the primary and secondary circuit. The pulse

transformer with closed magnetic core has the largest effective coupling coefficient (close to 1) in contrast to Tesla transformer and air-core transformer. Under the condition of large coupling coefficient, the transformer in Fig. 22(a) can be decomposed as Fig. 22(b) shows. L_μ , L_{lp} and L_{ls} are defined in (5), (11) and (14), respectively. Define the turns ratio of transformer as $n_s=(N_2/N_1)$. C_2 , L_{ls} , L_{sl} , R_s and i_s in the secondary circuit also can be equated into the primary circuit as C'_2 , L'_{ls} , L'_{sl} , R'_s and i'_s . The equating law are as $C'_2=C_2n_s^2$, $L'_{ls}=L_{ls}/n_s^2$, $L'_{sl}=L_{sl}/n_s^2$, $R'_s=R_s/n_s^2$, and $i'_s=i_s n_s$. The initial voltage of C_1 and C_2 are as U_0 and 0 respectively.

The voltages of C_1 and C_2 are $U_{c1}(t)$ and $U_{c2}(t)$, respectively. According to Fig. 22(a), the circuit equations of HES module are as

$$\begin{cases} U_0 - \frac{\int i_p(t)}{C_1} = R_p i_p(t) + (L_\mu + L_{lp} + L_{pl}) \frac{di_p(t)}{dt} - M \frac{di_s(t)}{dt} \\ M \frac{di_p(t)}{dt} = (L_\mu n_s^2 + L_{ls} + L_{sl}) \frac{di_s(t)}{dt} + R_s i_s(t) + \frac{\int i_s(t)}{C_2} \end{cases} \quad (45)$$

In view of Fig. 22(b), the circuit equations of HES module can also be established as

$$\begin{cases} (L_\mu + L_{pl} + L_{lp}) \frac{d^2 i_p}{dt^2} + R_p \frac{di_p}{dt} + \frac{i_p}{C_1} = L_\mu \frac{d^2 i_s}{dt^2} \\ (L_\mu + L_{sl} + L'_{ls}) \frac{d^2 i'_s}{dt^2} + R'_s \frac{di'_s}{dt} + \frac{i'_s}{C'_2} = L_\mu \frac{d^2 i_p}{dt^2} \end{cases} \quad (46)$$

The initial conditions are as $i_p(0)=0$, $i_s(0)=0$, $U_{c1}(0)=U_0$ and $U_{c2}(0)=0$. In view of that $i_p(t)=-C_1 dU_{c1}(t)/dt$ and $i_s(t)=-C_2 dU_{c2}(t)/dt$, Equations in (45) can be simplified as

$$\begin{cases} \frac{d^2 U_{c1}(t)}{dt^2} + 2\alpha_p \frac{dU_{c1}(t)}{dt} + \omega_p^2 U_{c1} - k_p \frac{d^2 U_{c2}(t)}{dt^2} = 0 \\ \frac{d^2 U_{c2}(t)}{dt^2} + 2\alpha_s \frac{dU_{c2}(t)}{dt} + \omega_s^2 U_{c2} - k_s \frac{d^2 U_{c1}(t)}{dt^2} = 0 \end{cases} \quad (47)$$

In (47), ω_p and ω_s are defined as the resonant angular frequencies in primary and secondary circuits, while k_p and k_s are defined as the coupling coefficients of the primary and secondary circuits respectively. These parameters are presented as

$$\begin{cases} \omega_p^2 = 1 / [(L_1 + L_{pl})C_1], \omega_s^2 = 1 / [(L_2 + L_{sl})C_2] \\ \alpha_p = R_p / 2(L_1 + L_{pl}), \alpha_s = R_s / [2C_2(L_2 + L_{sl})] \\ k_p = MC_2 / C_1(L_1 + L_{pl}), k_s = MC_1 / C_2(L_2 + L_{sl}) \end{cases} \quad (48)$$

Define the effective coupling coefficient of the HES module based on transformer charging as k , and the quality factors of the primary and secondary circuits as Q_1 and Q_2 respectively. k , Q_1 and Q_2 are presented as

$$\left\{ \begin{aligned} k^2 &= \frac{M^2}{(L_1 + L_{pl})(L_2 + L_{sl})} = \frac{L_\mu^2}{(L_\mu + L_{lp} + L_{pl})n_s^2(L_\mu + L_{ls} + L_{sl})} = k_p k_s \\ Q_1 &= \frac{\omega_p(L_1 + L_{pl})}{R_p}, Q_2 = \frac{\omega_s(L_2 + L_{sl})}{R_s} \end{aligned} \right. \quad (49)$$

Equations (47) have general forms of solution as $U_{c1}(t)=D_1e^{xt}$ and $U_{c2}(t)=D_2e^{xt}$. Through substituting the general solutions into (47), linear algebra equations of the coefficients D_1 and D_2 are obtained. The characteristic equation of the linear algebra equations obtained is calculated as

$$(1 - k^2)x^4 + 2(\alpha_p + \alpha_s)x^3 + (\omega_p^2 + 4\alpha_p\alpha_s + \omega_s^2)x^2 + 2(\alpha_p\omega_p^2 + \alpha_s\omega_s^2)x + \omega_p^2\omega_s^2 = 0. \quad (50)$$

x in the characteristic equation (50) represents the characteristic solution. As a result, x , D_1 and D_2 should be calculated before the calculations of $U_{c1}(t)$ and $U_{c2}(t)$. Obviously, the characteristic solution x can be obtained through the solution formula of algebra equation (50), but x will be too complicated to provided any useful information. In order to reveal the characteristics of the HES module in a more informative way, two methods are introduced to solve the characteristic equation (50) in this section.

4.1. The lossless method

The first method employs lossless approximation. That's to say, the parasitic resistances in the HES module are so small that they can be ignored. So, the HES module has no loss. Actually in many practices, the "no loss" approximation is reasonable. As a result, equation (50) can be simplified as

$$(1 - k^2)x^4 + (\omega_p^2 + \omega_s^2)x^2 + \omega_p^2\omega_s^2 = 0. \quad (51)$$

In (51), it is easy to get the two independent characteristic solutions defined as x_{\pm} . $U_{c1}(t)=D_1e^{x_+t}$ and $U_{c2}(t)=D_2e^{x_-t}$ can also be calculated combining with the initial circuit conditions. Finally, the most important four characteristic parameters such as $U_{c1}(t)$, $U_{c2}(t)$, $i_p(t)$ and $i_s(t)$, are all obtained as

$$\left\{ \begin{aligned} U_{c1}(t) &= \frac{(1+T)L_\mu - L_\Sigma}{(1+T)^2L_\mu - TL_\Sigma} U_0 \left[\frac{(1+T)L_\mu}{(1+T)L_\mu - L_\Sigma} \cos(\omega_+t) + T \cos(\omega_-t) \right] \\ U_{c2}(t) &= \frac{(1+T)L_\mu - L_\Sigma}{(1+T)^2L_\mu - TL_\Sigma} \sqrt{\frac{L_1 + L_{pl}}{L_2 + L_{sl}}} \frac{C_1 U_0}{k C_2} [\cos(\omega_+t) - \cos(\omega_-t)] \\ i_p(t) &= \frac{(1+T)L_\mu - L_\Sigma}{(1+T)^2L_\mu - TL_\Sigma} C_1 U_0 \left[\frac{(1+T)L_\mu \omega_+}{(1+T)L_\mu - L_\Sigma} \sin(\omega_+t) + T \omega_- \sin(\omega_-t) \right] \\ i_s(t) &= \frac{(1+T)L_\mu - L_\Sigma}{(1+T)^2L_\mu - TL_\Sigma} \sqrt{\frac{L_1 + L_{pl}}{L_2 + L_{sl}}} \frac{C_1 U_0}{k} [\omega_+ \sin(\omega_+t) - \omega_- \sin(\omega_-t)] \end{aligned} \right. \quad (52)$$

In (52), L_{Σ} represents the sum of the parasitic inductances and leakage inductances, while ω_+ and ω_- stand for the two resonant angular frequencies existing in the HES module ($\omega_+ \gg \omega_-$). Parameters such as T , L_{Σ} , ω_+ and ω_- are as

$$\begin{cases} T \triangleq \omega_s^2 / \omega_p^2, L_{\Sigma} = L_{pl} + L_{lp} + (L_{ls} + L_{sl}) / n_s^2 \\ \omega_+^2 = \frac{1+T}{L_{\Sigma}C_1}, \quad \omega_-^2 = \frac{T}{(1+T)L_{\mu}C_1} \end{cases} \quad (53)$$

In (52), the voltages of energy storage capacitors have phase displacements in contrast to the currents. All of the voltage and current functions have two resonant angular frequencies as ω_+ and ω_- at the same time, which demonstrates that the HES module based on transformer with closed magnetic core is a kind of double resonant module. The input and output characteristics and the energy transferring are all determined by (52).

4.2. The “little disturbance” method

The “little disturbance” method was introduced to analyze the Tesla transformer with open core by S. D. Korovin in the Institute of High-Current Electronics (IHCE), Tomsk, Russia. Tesla transformer with open core has a different energy storage mode in contrast to the transformer with closed magnetic core. Tesla transformer mainly stores magnetic energy in the air gaps of the open core, while transformer with closed core stores magnetic energy in the magnetic core. So, the calculations for parameters of these two kinds of transformer are also different. However, the idea of “little disturbance” is still a useful reference for pulse transformer with closed core [24-25]. So, the “little disturbance” method is introduced to analyze the pulse transformer with closed magnetic core for HES module.

The “little disturbance” method employs two little disturbance functions Δx_{\pm} to rectify the characteristic equation (50) or (51). That’s to say, the previous characteristic solutions x_{\pm} are substituted by $x_{\pm} + \Delta x_{\pm}$. In HES module, the parasitic resistances which cause the energy loss still exist, though they are very small. So, the parasitic resistances also should be considered. Define j as unit of imaginary number, and variable x_j as $-jx/\omega_s$. Equation (50) can be simplified as

$$\left(x_j^2 - \frac{j}{Q_1\alpha^{\frac{1}{2}}}x_j - \frac{1}{\alpha}\right)\left(x_j^2 - \frac{j}{Q_2}x_j - 1\right) = k^2x_j^4 \quad (54)$$

Through substituting x_j by $x_{\pm} + \Delta x_{\pm}$ in (54), the characteristic equation of Δx_{\pm} can be obtained. If the altitude variables are ignored, the solutions of the characteristic equation of Δx_{\pm} are presented as

$$\left\{ \begin{array}{l} x_+ = \left[\frac{(1+T)L_\Sigma}{TL_\Sigma} \right]^{\frac{1}{2}}, \quad x_- = \left(\frac{1}{1+T} \right)^{\frac{1}{2}} \\ \frac{1}{\alpha} (x_\pm^2 - 1) + \frac{1}{Q_2} (x_\pm^2 - \frac{1}{\alpha}) \\ \Delta x_\pm = \frac{j \alpha^2 Q_1}{2 \cdot 2x_\pm^2(1-k^2) - 1 - \frac{1}{\alpha}} \end{array} \right. \quad (55)$$

The solutions of (50) are as $x = jx_i\omega_s = j(x_\pm + \Delta x_\pm)\omega_s$. Δx_\pm shown in (55) describes the damping effects of the parasitic resistances in the circuit. The two resonant angular frequencies ω_\pm are rectified as

$$\omega_\pm = x_\pm \omega_s, \quad \Delta \omega_\pm = \Delta x_\pm \omega_s. \quad (56)$$

Define two effective quality factors of the double resonant circuit of HES module as

$$Q_{eff+} = \frac{\omega_+}{2|\Delta\omega_+|} = \frac{\rho_1}{R_1 + R_2 / n_s^2}, \quad Q_{eff-} = \frac{\omega_-}{2|\Delta\omega_-|}. \quad (57)$$

$$\left\{ \begin{array}{l} U_{c1}(t) = G_1 e^{-\beta_+ t} \left[\cos(\omega_+ t) + \frac{\sin(\omega_+ t)}{2Q_{eff+}} \right] + G_2 e^{-\beta_- t} \left[\cos(\omega_- t) + \frac{\sin(\omega_- t)}{2Q_{eff-}} \right] \\ U_{c2}(t) = G_3 \left[e^{-\beta_+ t} \left(\cos(\omega_+ t) + \frac{\sin(\omega_+ t)}{2Q_{eff+}} \right) - e^{-\beta_- t} \left(\cos(\omega_- t) + \frac{\sin(\omega_- t)}{2Q_{eff-}} \right) \right] \\ i_p(t) = -C_1 \left\{ G_1 e^{-\beta_+ t} \left[-\beta_+ \left(\cos(\omega_+ t) + \frac{\sin(\omega_+ t)}{2Q_{eff+}} \right) + \omega_+ \left(\frac{\cos(\omega_+ t)}{2Q_{eff+}} - \sin(\omega_+ t) \right) \right] + \right. \\ \left. G_2 e^{-\beta_- t} \left[-\beta_- \left(\cos(\omega_- t) + \frac{\sin(\omega_- t)}{2Q_{eff-}} \right) + \omega_- \left(\frac{\cos(\omega_- t)}{2Q_{eff-}} - \sin(\omega_- t) \right) \right] \right\} \\ i_s(t) = -C_2 G_3 \left[-\beta_+ e^{-\beta_+ t} \left(\cos(\omega_+ t) + \frac{\sin(\omega_+ t)}{2Q_{eff+}} \right) + \omega_+ e^{-\beta_+ t} \left(\frac{\cos(\omega_+ t)}{2Q_{eff+}} - \sin(\omega_+ t) \right) + \right. \\ \left. \beta_- e^{-\beta_- t} \left(\cos(\omega_- t) + \frac{\sin(\omega_- t)}{2Q_{eff-}} \right) - \omega_- e^{-\beta_- t} \left(\frac{\cos(\omega_- t)}{2Q_{eff-}} - \sin(\omega_- t) \right) \right] \end{array} \right. \quad (58)$$

In (57), ρ_1 represents the characteristic impedance of the resonant circuit, and $\rho_1 = [L_\Sigma(1+T)/C_1]^{1/2}$. According to (55), the general solutions of (49) ($U_{c1}(t) = D_1 e^{x_+ t}$ and $U_{c2}(t) = D_2 e^{x_- t}$) are clarified. When the initial circuit conditions are considered, the important four characteristic parameters such as $U_{c1}(t)$, $U_{c2}(t)$, $i_p(t)$ and $i_s(t)$ are obtained as (58). In (58), $\beta_\pm = |\Delta\omega_\pm| = |\Delta x_\pm| \omega_s$, coefficients such as G_1 , G_2 and G_3 are defined as

$$G_1 = \frac{x_-^2(x_+^2 - 1)}{x_+^2 - x_-^2} U_0, \quad G_2 = \frac{x_-^2 x_+^2 T}{x_+^2 - x_-^2} U_0, \quad G_3 = \frac{x_-^2 x_+^2}{x_+^2 - x_-^2} \sqrt{\frac{L_1 + L_{pl}}{L_2 + L_{sl}}} \frac{C_1}{kC_2} U_0. \quad (59)$$

From (58), all of the voltage and current functions have two resonant frequencies. In many situations of practice, the terms in (58) which include $\cos(\omega \cdot t)$ and $\sin(\omega \cdot t)$ can be ignored, as $\omega_+ \gg \omega_-$ and $\beta_+ \gg \beta_-$. The resonant currents $i_p(t)$ and $i_s(t)$ in primary and secondary circuit are almost in synchronization as shown in Fig. 23, and their resonant phases are almost the same. The first extremum point of $U_{c2}(t)$ defined as $(t_m, U_{c2}(t_m))$ corresponds to the maximum charge voltage and peak charge time of C_2 . Of course, t_m also corresponds to the time of minimum voltage on C_1 . That's to say, t_m is a critical time point which corresponds to maximum energy transferring. As $i_s(t) = -C_2 dU_{c2}(t)/dt$, $i_s(t)$ gets close to 0 when $t = t_m$. If $\omega_+ \gg \omega_-$, the maximum charge voltage and peak charge time of C_2 are calculated as

$$\begin{cases} t_m = \frac{\pi}{\omega_+} = \pi \left(\frac{L_2 C_1}{1+T} \right)^{\frac{1}{2}} \\ U_{c2}(t_m) = -G_3 \left(1 + \exp\left(-\frac{\pi}{2Q_{eff+}}\right) \right) \end{cases} \quad (60)$$

Obviously, when the switch of C_1 in Fig.2 opens while the switch of C_2 closes both at t_m , the energy stored in C_2 reaches its maximum, and the energy delivered to the terminal load also reaches the maximum. This situation corresponds to the largest efficiency of energy transferring of the HES module. Of course, if the switch in Fig. 22(a) is closed all the time, the HES module acts in line with the law shown in (58). The energy stored in C_1 is transferred to transformer and capacitor C_2 , then the energy is recycled from C_2 and transformer to C_1 excluding the loss, and then the aforementioned courses operate repetitively. Finally, all of the energy stored in C_1 becomes loss energy on the parasitic resistors, and the resonances in the HES module die down.

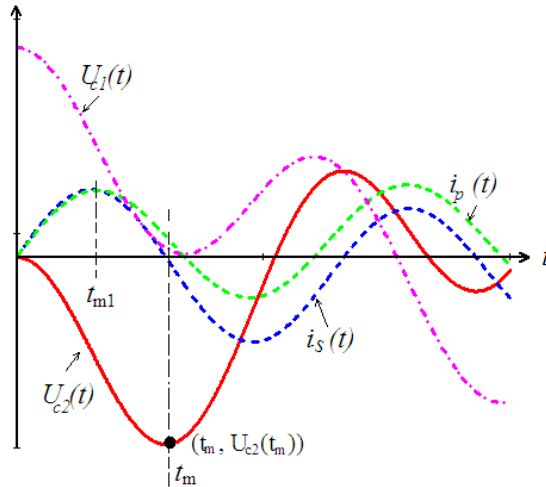


Figure 23. Typical theoretical waveforms of the output parameters of HES module based on pulse transformer charging, according to the “little disturbance” method

Under the condition $\omega \gg \omega_+$, the peak time and the peak current of $i_p(t)$ are calculated as

$$\left\{ \begin{array}{l} t_{m1} \approx \frac{\pi}{2\omega_+} = \frac{\pi}{2} \left(\frac{L_\Sigma C_1}{1+T} \right)^{\frac{1}{2}} \\ i_p(t_{m1}) = G_1 C_1 \omega_+ \left(1 + \frac{1}{4Q_{eff+}^2} \right) \exp\left(-\frac{\pi}{4Q_{eff+}} \right) \end{array} \right. \quad (61)$$

Usually, semiconductor switch such as thyristor or IGBT is used as the controlling switch of C_1 . However, these switches are sensitive to the parameters of the circuit such as the peak current, peak voltage, and the raising ratios of current and voltage. The raising ratio of $U_{c1}(t)$ and $i_p(t)$ ($dU_{c1}(t)/dt$ and $di_p(t)/dt$) can also be calculated from (58), which provides theoretical instructions for option of semiconductor switch in the HES module.

Actually, the efficiency of energy transferring is also determined by the charge time of C_2 in practice. Define the charge time of C_2 as t_c , the maximum efficiency of energy transferring on C_2 as η_a , and the efficiency of energy transferring in practice as η_e . If the core loss of transformer is very small, the efficiencies of HES module based on pulse transformer charging are as

$$\eta_a = \frac{\frac{1}{2} C_2 U_{c2}^2(t_m)}{\frac{1}{2} C_1 U_0^2} = \frac{C_1}{k^2 C_2} \frac{L_1 + L_{pl}}{L_2 + L_{sl}} \left(\frac{(1+T)L_\mu - L_\Sigma}{(1+T)^2 L_\mu - TL_\Sigma} \right)^2, \quad \eta_e = \frac{\frac{1}{2} C_2 U_{c2}^2(t_c)}{\frac{1}{2} C_1 U_0^2} \leq \eta_a. \quad (62)$$

Actually, t_c corresponds to the time when S_2 closes in Fig. 2.

5. Magnetic saturation of pulse transformer and loss analysis of HES

5.1. Magnetic saturation of pulse transformer with closed magnetic core

Transformers with magnetic core share a communal problem of magnetic saturation of core. The pulse transformer with closed magnetic core consists of the primary windings (N_1 turns) and the secondary windings (N_2 turns), and it works in accordance with the hysteresis loop shown in Fig.24. Define the induced voltage of primary windings of transformer as $U_p(t)$, and the primary current as $i_p(t)$. If the input voltage $U_p(t)$ increases, the magnetizing current in primary windings also increases, leading to an increment of the magnetic induction intensity B generated by $i_p(t)$. When B increases to the level of the saturation magnetic induction intensity B_s , dB/dH at the working point (H_0, B_0) decreases to 0 and the relative permeability μ_r of magnetic core decreases to 1. Under this condition, magnetic characteristics of the core deteriorate and magnetic saturation occurs. Once the magnetic saturation occurs, the transformer is not able to transfer voltage and energy. So, it's an important issue for a stable transformer to improve the saturation characteristics of magnetic core and keep the input voltage $U_p(t)$ at a high level simultaneously.

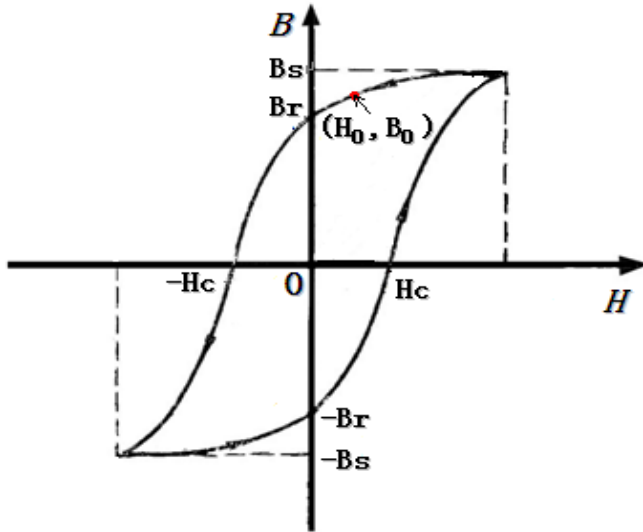


Figure 24. Typical hysteresis loop of magnetic core of pulse transformer

The total magnetic flux in the magnetic core is Φ_0 defined in (4). According to Faraday’s law, $U_p(t)=d\Phi_0 /dt$. Define the allowed maximum increment of B in the hysteresis loop as ΔB_{max} , and the corresponding maximum increment of Φ_0 as $\Delta\Phi$. Obviously, $\Delta B_{max}=B_s-(-B_r)$ and $\Delta\Phi=N_1\Delta B_{max}SK_T$, while parameters such as B_r , S and K_T are defined before (3). So, the relation between S and the voltage second product of core is presented as

$$S = \frac{\int_0^{t_c} U_p(t)dt}{N_1\Delta B_{max}K_T} = \frac{\int_0^{t_c} U_s(t)dt}{N_2\Delta B_{max}K_T} \tag{63}$$

As parameters such as ΔB_{max} , N_1 , N_2 , S and K_T are unchangeable and definite in an already produced transformer, the charge time t_c defined in (62) can not be long at random. Otherwise, $\int_0^{t_c} U_p(t)dt > N_1\Delta B_{max}K_T S$, the core saturates and the transformer is not able to transfer energy. That’s to say, (63) just corresponds to the allowed maximum charge time without saturation. If the allowed maximum charge time is defined as t_s , $\int_0^{t_s} U_p(t)dt = N_1\Delta B_{max}K_T S$.

According to (63), some methods are obtained to avoid saturation of core as follows. Firstly, ΔB_{max} and K_T of the magnetic material should be as large as possible. Secondly, the cross-

section area of core should be large enough. Thirdly, the turn number of transformer windings (N_1) should be enhanced. Fourthly, the charge time t_c of transformer should be restricted effectively. Lastly, the input voltage $U_p(t)$ of transformer should decrease to a proper range.

Generally speaking, it is quite difficult to increase ΔB_{\max} and K_T . The increment of N_1 leads to decrement of the step-up ratio of transformer. And the decrement of $U_p(t)$ leads to low voltage output from the secondary windings. As a result, the common used methods to avoid saturation of core include the increasing of S and decreasing the charge time t_c through proper circuit designing. Finally, the minimum cross-section design (S_{\min}) of magnetic core in transformer should follow the instruction as shown in (64).

$$S \geq S_{\min} = \frac{\int_0^{t_s} U_p(t) dt}{N_1 \Delta B_{\max} K_T} \geq \frac{\int_0^{t_c} U_p(t) dt}{N_1 \Delta B_{\max} K_T} = \frac{\int_0^{t_c} U_s(t) dt}{N_2 \Delta B_{\max} K_T}. \quad (64)$$

In (64), $U_p(t)$ and $U_s(t)$ can be substituted by $U_{c1}(t)$ and $U_{c2}(t)$ calculated in (52) or (58). Moreover, small air gaps can be introduced in the cross section of magnetic core to improve the saturation characteristics, which has some common features with the Tesla transformer with opened magnetic core. Reference [40] explained the air-gap method which is at the costs of increasing leakage inductances and decreasing the coupling coefficient.

5.2. Loss analysis of HES

The loss is a very important issue to estimate the quality of the energy transferring module. In Fig. 22(a), the main losses in the HES module based on pulse transformer charging include the resistive loss and the loss of magnetic core of transformer. The resistive loss in HES module consists of loss of wire resistance, loss of parasitic resistance of components, loss of switch and loss of leakage conductance of capacitor. Energy of resistive loss corresponds to heat in the components. The wire resistance is estimated in (27), and the switch resistance and leakage conductance of capacitor are provided by the manufacturers. According to the currents calculated in (58), the total resistive loss defined as ΔW_R can be estimated conveniently. In this section, the centre topic focuses on the loss of magnetic core of transformer as follows.

5.2.1. Hysteresis loss analysis

In the microscope of the magnetic material, the electrons in the molecules and atoms spin themselves and revolve around the nucleuses at the same time. These two types of movements cause magnetic effects of the material. Every molecule corresponds to its own magnetic dipole, and the magnetic dipole equates to a dipole generated by a hypothetic molecule current. When no external magnetic field exists, large quantities of magnetic dipoles of molecule current are in random distribution. However, when external magnetic

field exists, the external magnetic field has strong effect on these magnetic dipoles in random distribution, and the dipoles turn to the same direction along the direction of external magnetic field. The course is called as magnetizing, in which a macroscopical magnetic dipole of the material is formed. Obviously, magnetizing course of the core consumes energy which comes from capacitor C_1 in Fig. 2, and this part of energy corresponds to the hysteresis loss of core defined as W_{loss1} .

Define the electric field intensity, electric displacement vector, magnetic field intensity and magnetic induction intensity in the magnetic core as \vec{E} , \vec{D} , \vec{H} and \vec{B} respectively. The total energy density of electromagnetic field $W = \int (\vec{E} \cdot \partial \vec{D} / \partial t + \vec{H} \cdot \partial \vec{B} / \partial t) dt$. As the energy density of electric field is the same as which of magnetic field, the total energy density W in isotropic material can be simplified as

$$W = (\vec{E} \cdot \vec{D} + \vec{H} \cdot \vec{B}) / 2 = \vec{H} \cdot \vec{B} \quad \text{or} \quad dW = H dB. \quad (65)$$

The magnetizing current which corresponds to W_{loss1} is a small part of the total current $i_p(t)$ in primary windings. Define the magnetizing current as $I_m(t)$, the average length of magnetic pass as $\langle l_c \rangle$, and the total volume of magnetic core as V_m . According to the Ampere's circuital law and Faraday's law,

$$H = N_1 I_m(t) / \langle l_c \rangle, \quad dB = -U_p(t) dt / N_1 S K_T. \quad (66)$$

According to (65) and (66), the hysteresis loss of magnetic core of transformer is obtained as

$$W_{\text{loss1}} = \int_0^{t_c} \frac{|U_p(t) I_m(t)| V_m}{\langle l_c \rangle S K_T} dt \quad (67)$$

In some approximate calculations, the loss energy density is equivalent to the area enclosed by the hysteresis loop. If the coercive force of the loop is H_c , $W_{\text{loss1}} \approx 2H_c B_s V_m$.

5.2.2. Eddy current loss analysis

When transformer works under high-frequency conditions, the high-frequency current in transformer windings induces eddy current in the cross section of magnetic core. Define the eddy current vector as \vec{j} , magnetic induction intensity of eddy current as \vec{B}' , magnetic field intensity of eddy current as \vec{H}' , magnetic induction intensity of $i_p(t)$ as \vec{B}_0 , and magnetic field intensity of $i_p(t)$ as \vec{H}_0 . As shown in Fig. 25, the direction of \vec{j} is just inverse to the direction of $i_p(t)$, so the eddy current field \vec{B}' weakens the effect of \vec{B}_0 . The eddy current heats the core and causes loss of transformer, and it should be eliminated by the largest extent when possible.

In order to avoid eddy current loss, the magnetic core is constructed by piled sheets in the cross section as Fig. 25 shows. Usually, the sheet is covered with a thin layer of insulation

material to prevent eddy current. However, the high-frequency eddy current has “skin effect”, and the depth of “skin effect” defined as δ is usually smaller than the thickness h of the sheet. As a result, the eddy current still exists in the cross section of core. Cartesian coordinates are established in the cross section of core as shown in Fig. 25, and the unit vectors are as \bar{e}_x , \bar{e}_y and \bar{e}_z . To a thin sheet, its length (\bar{e}_z) and width (\bar{e}_y) are both much larger than the thickness h (\bar{e}_x). So, approximation of infinite large dimensions of sheet in \bar{e}_y and \bar{e}_z directions is reasonable. That's to say, $\partial/\partial y=0$ and $\partial/\partial z=0$. The “little disturbance” theory aforementioned before still can be employed to calculate the field \bar{B}' generated by eddy current \bar{j}' .

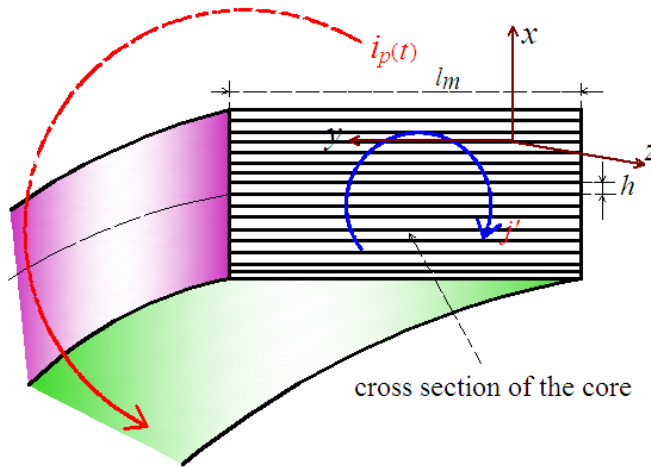


Figure 25. Distribution of eddy current in the cross section of toroidal magnetic core

The total magnetic induction intensity in the core is as $\bar{B} = \bar{B}_0 + \bar{B}' = (B_0 - B')\bar{e}_z$, and $B' \ll B_0$. \bar{B}' generated by eddy current can be viewed as the variable of “little disturbance”. According to Maxwell equations,

$$\begin{cases} \nabla \times \vec{E} = -\partial \vec{B} / \partial t \\ \nabla \times \vec{H} = \nabla \times (\vec{H}_0 + \vec{H}') = \vec{j}' + \partial \vec{D} / \partial t \end{cases} \quad (68)$$

From (68), it is easy to obtain the formula $\partial E_y / \partial x \approx -\partial B_0 / \partial t$, while (E_x, E_y, E_z) and (H_x, H_y, H_z) corresponds to vectors \vec{E} and \vec{H} . Through integration,

$$\vec{E}(x) = -x(\partial B_0 / \partial t) \vec{e}_y, \quad -h/2 \leq x \leq h/2. \quad (69)$$

Define the conductivity of the sheet in magnetic core as σ . From the second equation in (68), $(-\partial H'_z / \partial x) \vec{e}_y = \vec{j}' = \sigma \vec{E}$. It demonstrates that infinitesimal conductivity is the key factor to prevent eddy current. When working frequency is f , the depth of “skin effect” of the sheet is calculated as $\delta = (\pi f \mu \sigma)^{-1/2}$. According to (69), the “little disturbance” field of eddy current in isotropic magnetic material is presented as

$$\vec{H}'(x) = \frac{\sigma x^2}{2} \frac{\partial B_0}{\partial t} \vec{e}_z, \quad \vec{B}'(x) = \frac{\mu_0 \mu_r \sigma x^2}{2} \frac{\partial B_0}{\partial t} = \frac{1}{\omega} \left(\frac{x}{\delta}\right)^2 \frac{\partial B_0}{\partial t} \vec{e}_z, \quad \left(-\frac{h}{2} \leq x \leq \frac{h}{2}\right). \quad (70)$$

Through averaging the field along the thickness direction (\vec{e}_x) of sheet,

$$\vec{H}'' = \frac{\sigma h^2}{24} \frac{\partial B_0}{\partial t}, \quad \vec{B}'' = \frac{1}{12\omega} \left(\frac{h}{\delta}\right)^2 \frac{\partial B_0}{\partial t}. \quad (71)$$

As the electric energy and magnetic energy of the eddy current field are almost the same, the eddy current loss defined as W_{loss2} is calculated as

$$W_{\text{loss2}} = \int_0^t dt \iiint_V \vec{B}'' \vec{H}'' dV = \frac{\sigma h^2}{288\omega} \left(\frac{h}{\delta}\right)^2 V_m \int_0^t \left(\frac{\partial B_0}{\partial t}\right)^2 dt \quad (72)$$

From (72), W_{loss2} is proportional to the conductivity σ of the core, and it is also proportional to $(h/\sigma)^2$. As a result, W_{loss2} can be limited when $h \ll \delta$.

5.2.3. Energy efficiency of the HES module

As to the HES module based on transformer charging shown in Fig. 22(a), the energy loss mainly consists of ΔW_R , W_{loss1} and W_{loss2} . Total energy provided from C_1 is as $W_0 = \frac{1}{2} C_1 U_0^2$.

In practice, the energy stored in C_1 can not be transferred to C_2 completely, though the loss of the module is excluded. In other words, residue energy defined as W_{or} exists in C_1 . Define the allowed maximum efficiency of energy transferring from C_1 to C_2 as η_{max} . So, η_{max} of the HES module is as

$$\eta_{\max} = \frac{W_0 - (\Delta W_R + W_{\text{loss1}} + W_{\text{loss2}}) - W_{0r}}{W_0}. \quad (73)$$

From (62), η_a , η_e and η_{\max} have relation as $\eta_e \leq \eta_a \leq \eta_{\max}$.

Author details

Yu Zhang* and Jinliang Liu

College of Opto-Electronic Science and Engineering, National University of Defense Technology, Changsha, China

Acknowledgement

This work was supported by the National Science Foundation of China under Grant No.51177167. It's also supported by the Fund of Innovation, Graduate School of National University of Defense Technology under Grant No.B100702.

6. References

- [1] Bialasiewicz J T (2008) Renewable energy systems with photovoltaic power generators: operation and modeling. *IEEE Transactions on Industrial Electronics*, 55(7): 2752-2758.
- [2] Anderson M D and Carr D S (1993) Battery energy storage technologies. *Proceedings of the IEEE*, 81(3): 475-479.
- [3] Schempp E and Jackson W D (1996) Systems considerations in capacitive energy storage. *Energy Conversion Engineering Conference*, 2: 666-671.
- [4] Beverly R E and Campbell R N (2010) A 1MV, 10kJ photo-triggered Marx generator. *IEEE Power Modulator and High-Voltage Conference*: 560-563.
- [5] Lehmann M (2010) High energy output Marx generator design. *IEEE Power Modulator and High-Voltage Conference*: 576-578.
- [6] Simon E and Bronner G (1967) An inductive energy storage system using ignitron switching. *IEEE Transactions on Nuclear Science*, 14(5): 33-40.
- [7] Gorbachev K V, Nesterov E V, Petrov V Yu, and Chernykh E V (2009) A helical-radial magnetic cumulation fast-growing current pulse generator. *Instruments and Experimental Technology*, 52(1): 58-64.
- [8] Doinikov N I, Druzhinin A S, Krivchenkov Yu M (1992) 900MJ toroidal transformer-type inductive energy storage. *IEEE Transactions on Magnetics*, 28(1): 414-417.

* Corresponding Author

- [9] Masugata K, Saitoh H, Maekawa H (1997) Development of high voltage step-up transformer as a substitute for a Marx generator. *Review of Scientific Instruments*, 68(5): 2214-2220.
- [10] Bushlyakov A I, Lyubutin S K, Ponomarev A V (2006) Solid-state SOS-based generator providing a peak power of 4 GW. *IEEE Transaction on Plasma Science*, 34(5): 1873-1878.
- [11] Rukin S, Lyubutin S, Ponomarev A (2007) Solid-state IGBT/SOS-based generator with 100-kHz pulse repetition frequency. *IEEE Pulsed Power Conference*: 861-864.
- [12] Korovin S D, Kurkan I K, Loginov S V, (2003) Decimeter-band frequency-tunable sources of high-power microwave pulses. *Laser and Particle Beams*, 21: 175-185.
- [13] Morton D, Weidenheimer D, Dasilva T, (2005) Performance of an advanced repetitively pulsed electron beam pumped KrF laser driver. *IEEE Pulsed Power Conference*: 1290-1293.
- [14] Sethian J D, Myers M, Smith I D, (2000) Pulsed power for a rep-rate, electron beam pumped KrF laser. *IEEE Transactions on Plasma Science*, 28(5): 1333-1337.
- [15] Sarkar P, Braidwoody SW, Smith I R, (2005) A compact battery-powered 500 kV pulse generator for UWB radiation. *IEEE Transactions on Plasma Science*, 33(5): 1306-1309.
- [16] Mesyats G A, Korovin S D, Rostov V V, Shpak V G, and Yalandin M I, (2004) The RADAN series of compact pulsed power generators and their applications. *Proceedings of the IEEE*, 92(7): 1166-1178.
- [17] Krasik Y E, Grinenko A, Sayapin A and Efimov S, (2008) Underwater electrical wire explosion and its applications. *IEEE Transactions on Plasma Science*, 36(2): 423-434.
- [18] Boeuf J P, (2003) Plasma display panel: physics, recent developments and key issues. *J. Physics D: Appl Phys*, 36(6): 53-79.
- [19] Choi Y W, Jeong I W, Rim G H, (2002) Development of a magnetic pulse compression modulator for flue gas treatment. *IEEE Transactions on Plasma Science*, 30(5): 1632-1636.
- [20] Rossi J O and Ueda M, (2006) A 100kV/200A Blumlein pulser for high-energy plasma implantation. *IEEE Transactions on Plasma Science*, 34(5): 1766-1770.
- [21] Kamase Y, Shimizu M, Nagahama T, (1993) Erosion of spark of square wave high-voltage source for ozone generation. *IEEE Transactions on industry applications*, 29(4): 793-797.
- [22] Gaudreau M P J, Hawkey T, Petry J and Kempkes M A, (2001) A solid state pulsed power system for food processing. *Digest of Technical Papers: Pulsed Power Plasma Science*: 1174-1177.
- [23] Gundersen M, Kuthi A, Behrend M and Vernier T, (2004) Bipolar nanosecond pulse generation using transmission lines for cell electro-manipulation. *Power Modulator Symposium and High-Voltage Workshop Conference*: 224-227.

- [24] Zhang Y, Liu J L, Cheng X B, (2010) Output Characteristics of a Kind of High-Voltage Pulse Transformer with Closed Magnetic Core. *IEEE Transactions on Plasma Science*, 38(4): 1019-1027.
- [25] Zhang Y, Liu J L, Cheng X B, (2010) A compact high voltage pulse generator based on pulse transformer with closed magnetic core. *Review of Scientific Instruments*, 81(3): 033302.
- [26] Rohwein G J, Lawson R N, Clark M C (1991) A compact 200kV pulse transformer system. *Proceeding of the 8th IEEE Pulsed Power Conference*: 968-970.
- [27] Korovin S D, Gubanov V P, Gunin A V, Pegel I V and Stepchenko A S, (2001) Repetitive nanosecond high-voltage generator based on spiral forming line. *The 28th IEEE international Conference on Plasma Science*: 1249-1251.
- [28] Hurley W G and Wilcox D J, (1994) Calculation of leakage inductance in transformer windings. *IEEE Transactions on Power Electronics*, 9(1): 121-126.
- [29] Massarini A, Kazimierczuk M K, (1997) Self-capacitance of inductors. *IEEE Transactions on Power Electronics*, 12(4): 671-676.
- [30] Blache F, Keradec J P and Cogitore B, (1994) Stray capacitances of two winding transformers: equivalent circuit, measurements, calculation and lowering. *IEEE Pulsed Power Conference*: 1211-1217.
- [31] Grandi G, Kazimierczuk M K, Massarini A, Reggiani U, (1999) Stray capacitances of single-layer solenoid air-core inductors. *IEEE Transactions on Industry Applications*, 33(5): 1162-1168.
- [32] Mostafa A E, Gohar M K, (1953) Determination of voltage, current, and magnetic field distributions together with the self-capacitance, inductance and HF resistance of single-layer coils. *Proceedings of the I. R. E.*: 537-547.
- [33] Collins J A, (1990) an accurate method for modeling transformer winding capacitances. *IEEE Pulsed Power Conference*: 1094-1099.
- [34] Kino G S and Paik S F, (1962) Circuit Theory of Coupled Transmission System. *Journal of Applied Physics*, 33(10): 3002-3008.
- [35] Zhang Y, Liu J L, Fan X L, (2011) Characteristic Impedance and Capacitance Analysis of Blumlein Type Pulse forming Line Based on Tape Helix. *Review of Scientific Instruments*, 82(10): 104701.
- [36] Lord H W, (1971) Pulse transformer. *IEEE Transactions on Magnetics*, 7(1): 17-28.
- [37] Nishizuka N, Nakatsuyama M and Nagahashi H, (1989) Analysis of pulse transformer on distributed parameter theory. *IEEE Transactions on Magnetics*, 25(5): 3260-3262.
- [38] Redondo L M, Silva J F and Margato E, (2007) Pulse shape improvement in core-type high-voltage pulse transformers with auxiliary windings. *IEEE Transactions on Magnetics*, 43(5): 1973-1982.
- [39] Costa E M M, (2010) Resonance on coils excited by square waves: explaining Tesla transformer, *IEEE Transactions on Magnetics*, 46(5): 1186-1192.

- [40] Zhang Y, Liu J L, Fan X L, Zhang H B, Feng J H, (2012) Saturation and Pulse Response Characteristics of the Fe-Based Amorphous Core with Air Gap. *IEEE Transactions on Plasma Science*, 40(1): 90-97.

INTECH

INTECH